Eukaryotic initiation factor 4A3 inhibits Wnt/β-catenin signaling and regulates axis formation in zebrafish embryos

Bo Wang[1#], Xiaozhi Rong[1,2#*], Yumei Zhou[1], Yunzhang Liu[1], Jiqin Sun[1], Beibei Zhao[1], Bei Deng[1], Lei Lu[3], Ling Lu[1], Yun Li[1,2] and Jianfeng Zhou[1,2*]

[1]Key Laboratory of Marine Drugs (Ocean University of China), Chinese Ministry of Education, and School of Medicine and Pharmacy, Ocean University of China, 5 Yushan Road, Qingdao 266003, China. [2]Laboratory for Marine Drugs and Bioproducts, Pilot National Laboratory for Marine Science and Technology (Qingdao), Qingdao 266003, China; [3]Model Animal Research Center of Nanjing University and MOE Key Laboratory of Model Animals for Disease Study, 12 Xuefu Road, Pukou High-Tech Zone, Nanjing 210061, China.

[#]These authors contributed equally to this work.

[*]To whom correspondence should be addressed: Jianfeng Zhou, School of Medicine and Pharmacy, Ocean University of China, 5 Yushan Road, Qingdao 266003, China. Tel.: 86-532-82032957; Fax: 86-532-82032957; E-mail address: jfzhou@ouc.edu.cn; or, Xiaozhi Rong, School of Medicine and Pharmacy, Ocean University of China, 5 Yushan Road, Qingdao 266003, China. Tel.: 86-532-82032957; Fax: 86-532-82032957; E-mail address: rongxiaozhi@ouc.edu.cn

Keywords: EIF4A3, Wnt/β-catenin signaling, β-catenin, Lef/Tcf, zebrafish, axis formation

Abstract

A key step in the activation of canonical Wnt signaling is the interaction between β-catenin and Tcf/Lefs that forms the transcription activation complex and facilitates the expression of target genes. Eukaryotic initiation factor 4A3 (EIF4A3) is an ATP-dependent DEAD box-family RNA helicase and acts as a core subunit of the exon junction complex (EJC) to control a series of RNA posttranscriptional processes. In this study, we uncovered that EIF4A3 functions as a Wnt inhibitor by interfering with the formation of β-catenin/Tcf transcription activation complex. As Wnt stimulation increases, accumulated β-catenin displaces EIF4A3 from a transcriptional complex with Tcf/Lef, allowing the active complex to facilitate the expression of target genes. In zebrafish embryos, *eif4a3* depletion inhibited the development of the dorsal organizer and pattern formation of the anterior neuroectoderm by increasing Wnt/β-catenin signaling. Conversely, overexpression of *eif4a3* decreased Wnt/β-catenin signaling and inhibited the formation of the dorsal organizer before gastrulation. Our results reveal novel roles of EIF4A3 in the inhibition of Wnt signaling and the regulation of embryonic development in zebrafish.

Introduction

Wnt/β-catenin signaling plays pivotal roles in regulating embryogenesis in multicellular organisms, adult tissue homeostasis, regeneration, and stem cell pluripotency (Clevers and Nusse, 2012; MacDonald et al., 2009; Nusse and Clevers, 2017). Dysregulation of Wnt/β-catenin activity is associated with many human diseases, including congenital malformations, tumorigenesis, and various skeletal diseases (Clevers and Nusse, 2012; MacDonald et al., 2009; Nusse and Clevers, 2017; Regard et al., 2012). Wnt ligands bind to LRP5/6 and members of the frizzled family of transmembrane receptors, triggering a signaling cascade that inhibits GSK3 and leads to the stabilization of β-catenin. Stabilized β-catenin is translocated into the nucleus, where it forms a transcription activation complex with Tcf/Lefs to activate the transcription of Wnt target genes (MacDonald and He, 2012; MacDonald et al., 2009; Niehrs, 2012). Thus, in the Wnt/β-catenin pathway, the binding between β-catenin and Tcf/Lefs is a key step to form the transcription activation complex and stimulate transcription of Wnt target genes.

The developmental role of Wnt/β-catenin signaling in the formation of the dorsoventral and anteroposterior axes in multiple animal species has been well-documented (Hikasa and Sokol, 2013; Langdon and Mullins, 2011; Petersen and Reddien, 2009). For example, in zebrafish embryos, maternally provided β-catenin has an important role in the establishment of the dorsal organizer before gastrulation, while zygotic Wnt/β-catenin signaling promotes the ventrolateral mesodermal development to limit the organizer after the onset of gastrulation (Bellipanni et al., 2006; Lekven et al., 2001; Yan et al., 2018). In addition, zygotic Wnt/β-catenin signaling directs anteroposterior neural development (Baker et al., 2010; Erter et al., 2001; Lekven et al., 2001; Ramel et al., 2005).

Eukaryotic initiation factor 4A3 (EIF4A3; also known as DDX48) is a core component of the exon junction complexes (EJCs). The mammalian EJC contains four core subunits: EIF4A3, MAGOH, Y14 (also known as RBM8A), and MLN51 (also known as CASC3 or BTZ) (Le Hir et al., 2016; Linder and Jankowsky, 2011). All four proteins can shuttle between the nucleus and cytoplasm. EIF4A3, MAGOH, and Y14 are located in the nucleus, while MLN51 is mainly cytoplasmic (Le Hir et al., 2016). Within this complex, EIF4A3 acts as an ATP-dependent DEAD-box RNA helicase and serves as a platform for the EJC assembly. EIF4A3 is highly conserved in invertebrates and vertebrates, and possesses all conserved motifs defining the DEAD-box family of RNA helicases (Le Hir et al., 2016; Linder and Jankowsky, 2011; Shibuya et al., 2006). The EJC plays important roles in the posttranscriptional fate of mRNA, including pre-mRNA splicing (Michelle et al., 2012), export (Le Hir et al., 2001), stability (Gehring et al., 2005; Palacios et al., 2004), translation (Chazal et al., 2013; Nott et al., 2004), localization, and nonsense-mediated decay (Hachet and Ephrussi, 2004; Palacios et al., 2004). The EJC is involved in a variety of biological processes *in vivo*. For example, in *Drosophila*, the EJC is essential for the localization of *oskar* mRNA to the posterior pole of the oocyte and is required for the differentiation of the photoreceptor by maintaining *MAP Kinase* splicing (Ashton-Beaucage et al., 2010; Hachet and Ephrussi, 2004; Mohr et al., 2001; Newmark and Boswell, 1994; Palacios et al., 2004; Roignant and Treisman, 2010; van Eeden et al., 2001). Additionally, the *Drosophila* EJC

regulates the splicing of the cell polarity gene *dlg1* to control Wnt signaling (Liu et al., 2016). The depletion of Eif4a3 in *Xenopus* leads to full-body paralysis and defects in sensory neurons, pigment cells, and cardiac development. Knockdown of *magoh* or *Y14* resulted in a phenotype virtually identical to Eif4a3 morphant phenotype (Haremaki et al., 2010; Haremaki and Weinstein, 2012). Mice with haploinsufficiency for EJC subunits exhibit altered embryonic neurogenesis and microcephaly, while the genetic suppression of *p53* significantly rescues microcephaly in these mice (Mao et al., 2016; Mao et al., 2015; McMahon et al., 2014; Silver et al., 2010). Together, these observations from different organisms suggest that the *in vivo* effect of EIF4A3 is due to its function within the EJC. Recently, several studies have indicated that EIF4A3 is associated with Richieri-Costa-Pereira syndrome (RCPS) which is autosomal-recessive acrofacial dysostosis (Favaro et al., 2014; Favaro et al., 2011; Hsia et al., 2018). In this disease, genetic alterations cause a partial loss of function of EIF4A3; however, the underlying molecular mechanism is unknown (Favaro et al., 2014; Miller et al., 2017). Other than the cellular function of EIF4A3 in RNA processing and the developmental roles of EIF4A3 as a core subunit of the EJC complex, the physiological effects of EIF4A3 and its underlying mechanisms have, thus far, remained unclear.

In this study, we found that EIF4A3 functions as a novel binding partner of the β-catenin and Tcf as well as inhibits Wnt/β-catenin signaling. Mechanistic studies demonstrated that EIF4A3 interferes with the β-catenin and Tcf/Lefs transcription activation complex and suppresses the Wnt signaling activity. Wnt stimulation leads to accumulated β-catenin displace EIF4A3 from a transcriptional complex with Tcf/Lef, allowing the active transcription complex to facilitate the expression of target genes. Additionally, we found that Eif4a3 attenuates Wnt activity to promote dorsal development and anterior neuroectoderm pattern formation in zebrafish embryos. Thus, EIF4A3/Eif4a3 functions not only as a Wnt/β-catenin signaling repressor but also as a regulator of axis formation during zebrafish embryogenesis.

Results

EIF4A3/Eif4a3 inhibits Wnt/β-catenin signaling

To identify Wnt/β-catenin regulators in zebrafish, we performed a yeast two-hybrid assay with the β-catenin armadillo (ARM) region as bait to search a zebrafish one-cell stage cDNA library. We identified Eif4a3 as a candidate β-catenin binding partner. Zebrafish Eif4a3 shows a high degree of sequence identity with its human homolog EIF4A3 (Fig. S1A) (Shibuya et al., 2006). Using zebrafish embryos and cultured human cells, we first tested whether EIF4A3/Eif4a3 can regulate endogenous Wnt/β-catenin transcriptional activity both *in vivo* and *in vitro*. Forced expression of zebrafish *eif4a3* mRNA decreased the basal levels of Wnt reporter (TOPFlash) activity, rather than Bmp reporter (BRE) activity or Nodal/Tgfβ reporter (ARE) activity in zebrafish embryos in a dose-dependent manner (Fig. 1A). Likewise, human EIF4A3 exhibited similar effect on Wnt reporter activity in HEK293T cells (Fig. 1B). Therefore, we speculated that EIF4A3/Eif4a3 affects the Wnt/β-catenin pathway. Subsequently, we investigated the genetic interaction between EIF4A3/Eif4a3 and Wnt/β-catenin signals in zebrafish embryos and HEK293T cells. Wnt/β-catenin signal transduction is a multi-step process involving several molecular components, including Wnt ligands, β-catenin, and Tcf/Lef. Consistent with previously reported results, injection of *wnt3a*, constitutively active β-catenin (*β-catΔN*, β-catenin which lacks the first 45 residues in the

N-terminal region and translocates into the nucleus to interact with the transcription factor to activate target gene expression), or constitutively active Tcf7l1 (*vp16-tcf7l1ΔN*, a β-catenin-independent VP16-Tcf7l1 fusion protein that lacks the β-catenin-binding site) mRNAs in zebrafish embryos enhanced Wnt reporter activity at 6 hpf (hours post fertilization) (Fig. 1C, D, E) (Feng et al., 2012; Rong et al., 2014; Rong et al., 2017). Co-injection of *eif4a3* and *wnt3a*, *β-catΔN*, or *vp16-tcf7l1ΔN* mRNA diminished Wnt reporter activity induced by Wnt3a and β-CatΔN, but not by VP16-Tcf7l1ΔN in zebrafish embryos (Fig. 1C, D, E). Likewise, overexpression of EIF4A3 inhibited Wnt3a- and β-CatΔN-, but not VP16-Tcf7l1ΔN-induced Wnt activity in HEK293T cells (Fig. 1F, G, H). Similarly, injection of *wnt3a*, *β-catΔN*, or *vp16-tcf7l1ΔN* mRNA into zebrafish embryos resulted in a dorsalized phenotype at 12.5 hpf (Fig. 1I, J). Co-injection of *eif4a3* mRNA with *wnt3a*, *β-catΔN*, or *vp16-tcf7l1ΔN* mRNA blocked Wnt3a- and β-CatΔN-, but not VP16-Tcf7l1ΔN-induced dorsalizing activities in zebrafish embryos (Fig. 1I, J). Collectively, these data suggested that EIF4A3/Eif4a3 inhibits Wnt/β-catenin signaling and may act at the β-catenin level.

EIF4A3 interacts with β-CATENIN

To determine the molecular mechanism underlying Wnt inhibition by EIF4A3/Eif4a3, we first assessed whether EIF4A3 and β-CATENIN interact with each other by co-immunoprecipitation (co-IP) assays. Both exogenous and endogenous EIF4A3 and β-CATENIN were observed in a same complex in HEK293T cells (Fig. 2A, upper and middle panels). Likewise, the two endogenous proteins bound to each other under physiological conditions in developing zebrafish embryos (Fig. 2A, lower panel). A series of human EIF4A3 deletion mutants were generated based on the known conserved motifs (Fig. 2B, S1A) (Le Hir et al., 2016; Shibuya et al., 2006). A region comprised of residues aa 57-254 of EIF4A3, which corresponds to EIF4A3 DEAD domain 1, was required for its interaction with β-CATENIN (Fig. 2C). We next mapped the binding regions required for the interaction between EIF4A3 and β-CATENIN using a series of previously generated β-CATENIN truncation mutants (Lu et al., 2015). We observed that EIF4A3 bound to amino acids (aa) 1-318 on the truncated form of β-CATENIN rather than to aa 1-274 or any other shorter N-terminal truncations. Additionally, EIF4A3 bound to both aa 319-484 and aa 485-781 mutants (Fig. 2D, E). Hence, the binding region for EIF4A3 is within aa 275-781, which includes 4-12 armadillo (Arm) repeats as well as the transactivation activity domain of β-CATENIN. Thus, we concluded that β-CATENIN/β-catenin and EIF4A3/Eif4a3 bind to each other both in cultured human cells and zebrafish embryos.

EIF4A3 inhibits Wnt/β-catenin signaling by interfering with the β-CATENIN/TCF7L2 transcription activation complex, and Wnt stimulation promotes disassociation of EIF4A3 from the transcriptional complex

Given that the binding site for EIF4A3 on β-CATENIN largely overlaps with that for TCF/LEF (Polakis, 2012; Valenta et al., 2012), we speculated that EIF4A3 may compete with TCF/LEF for the binding site on β-CATENIN to prevent the interaction between β-CATENIN and TCF/LEF and interfere with the β-CATENIN/TCF complex. We first confirmed that EIF4A3 indeed localized in the nucleus of cultured HeLa cells (Fig 3A). We next employed a pull-down assay to test whether EIF4A3 can directly interact with β-CATENIN or TCF. As shown in Fig. 3B, purified GST-tagged EIF4A3 binds to β-CATENIN and to TCF7L2, suggesting that EIF4A3 directly interacts with β-CATENIN and TCF7L2. To further confirm

the interaction between TCF7L2 and EIF4A3, we used a series of domain deletion mutants of TCF7L2 to map the region of TCF7L2 that is responsible for EIF4A3 interaction by coimmunoprecipitation assays (Fig. 3C). When the HMG box was deleted, the resulting mutant of TCF7L2 did not bind to EIF4A3(Fig. 3D). Thus, the results suggested that HMG box of TCF7L2 is likely important for association with EIF4A3. Moreover, interaction of EIF4A3 with β-CATENIN and with TCF7L2 at endogenous level was further confirmed by coimmunoprecipitation assays in HEK293T cells (Fig. 3I-K, right panel, lane 5). Therefore, we conclude from these experiments that EIF4A3 associates with β-CATENIN and TCF7L2. In addition, endogenous EIF4A3 bound to the promoters of the Wnt target genes, such as *AXIN2*, *CCND1*, *DKK1*, *LEF1*, and *SP5L*, but not to *GAPDH* or *α-satellite* in HEK293T cells, as indicated by chromatin immunoprecipitation (ChIP)-PCR analysis (Fig. 3E).

Since EIF4A3 can interact with β-CATENIN and TCF7L2 as well as associate with the promoters of Wnt target genes, we hypothesized that EIF4A3 functions as an inhibitor protein that interferes with the formation of β-CATENIN/TCF complex. To test this hypothesis, we first examined the effect of EIF4A3 on transcriptional activity of the β-CATENIN/TCF complex in HCT116 cells, which harbor a mutant β-catenin allele and exhibit overactivated Wnt activity. When β-CatΔN and TCF7L2 were co-transfected into HCT116 cells along with different amounts of EIF4A3, β-CatΔN/TCF7L2-induced Wnt reporter activity was inhibited by EIF4A3 in a dose-dependent manner (Fig. 3F). We next performed a co-IP assay using HCT116 cells with co-transfected Flag-tagged β-CATENIN and Myc-tagged Tcf7l2 along with various doses of HA-tagged EIF4A3. The amounts of Tcf7l2 that co-immunoprecipitated with β-CATENIN decreased as the amounts of HA-tagged EIF4A3 that associated with β-CATENIN increased, along with increasing doses of EIF4A3 (Fig. 3G, left panel). Similarly, the amounts of endogenous TCF7L2 that co-precipitated with endogenous β-CATENIN also decreased as the amounts of HA-tagged EIF4A3 that associated with endogenous β-CATENIN increased, along with increasing doses of EIF4A3 (Fig. 3G, right panel). Since EIF4A3 associates with the promoters of the Wnt target genes in HEK293T cells which were regarded as a Wnt-off cell line, these results suggested that EIF4A3 likely competes with β-CATENIN for binding to TCF7L2 and interferes the formation of β-CATENIN/TCF7L2 transcriptional activator complex.

To test this possibility, HEK293T cells were treated with BIO, a small molecular compound that activates Wnt signaling by inhibiting GSK3β activity (Sato et al., 2004). Activated Wnt increased the ChIP signals of β-CATENIN on the promoters of Wnt target genes, including *AXIN2* and *DKK1*, to facilitate their expression in HEK293T cells (Choi et al., 2013; Wu et al., 2013). However, activated Wnt led to reduction of the ChIP signals of EIF4A3 on the promoters of *AXIN2* and *DKK1* genes (Fig. 3H), suggesting that EIF4A3 released from the promoters of these genes upon Wnt stimulation. In addition, treating cells with BIO activates the Wnt signaling pathway, as indicated by the increased levels of non-phospho (active) β-CATENIN (non-p-β-CATENIN); it does not, however, alter the expression level of EIF4A3 (Fig. 3I-K, left panels, compare lane 1 with lane 2). This result implied that activated Wnt has little effect on the stability of EIF4A3. Given that accumulated β-catenin binds to Lef/Tcf to form the transcription activation complex and activated Wnt signaling stimulates the release of EIF4A3 from the promoters of Wnt target genes, we speculate that accumulated β-catenin may displace EIF4A3 from the TCF7L2 complex at the promoters of Wnt target genes upon

Wnt stimulation. To test this speculation, we evaluated the binding among EIF4A3, β-CATENIN, and TCF7L2 under different Wnt activity by reciprocal co-IP assays. In agreement with previous results, Wnt activation increased the association of β-CATENIN with TCF7L2 (Fig. 3I and J, right panels, compare lane 5 with lane 8). Conversely, the associations of EIF4A3 with β-CATENIN and with TCF7L2 reduced simultaneously upon BIO treatment (Fig. 3I-K, right panels, compare lane 5 with lane 8). These findings suggested that accumulated β-CATENIN likely competes with EIF4A3 for binding to TCF7L2 and displaces EIF4A3 from a transcriptional complex with TCF7L2 under increased Wnt stimulation. Taken together, we proposed a role for EIF4A3 in Wnt/β-catenin signaling: EIF4A3 binds to β-CATENIN, or to TCF7L2 as well as associates with the promoters of Wnt target genes; β-CATENIN and EIF4A3 are mutually exclusive binding to TCF7L2; EIF4A3 would be displaced from a transcriptional complex with TCF7L2 by accumulated β-CATENIN upon Wnt stimulation, which allows the transcription activation complex to stimulate transcription of Wnt target genes (Fig. 3L).

Forced expression of Eif4a3 in zebrafish embryos limited dorsal development by inhibiting maternal β-catenin action and the inhibitory effect of Eif4a3 is ATPase-independent

We next determined the physiological relevance of *eif4a3* in zebrafish embryos. Forced expression of *eif4a3* in zebrafish embryos led to typically ventralized phenotypes at 24 hpf with a reduced head structure and enlarged ventral structure (Fig. 4A). The ventralizing effect of Eif4a3 was dose-dependent (Fig. 4B, upper panel). Human *EIF4A3* has a comparable ventralizing effect to that of zebrafish *eif4a3* (Fig. 4B, lower panel). The ventralizing effects of EIF4A3/Eif4a3 were investigated by performing whole-mount *in situ* hybridization (WISH) to examine the expression patterns of an anterior neuroectoderm marker, *otx2*, at the bud stage and a hematopoietic marker, *gata1*, in the blood island at 24 hpf. Overexpression of EIF4A3/Eif4a3 reduced the expression domain of *otx2* and enlarged the expression domain of *gata1* (Fig. 4C-F). Maternal β-catenin promotes the development of the dorsal organizer before gastrulation (Bellipanni et al., 2006; Yan et al., 2018). We, therefore, postulated that the ventralized phenotypes caused by the overexpression of EIF4A3/Eif4a3 might result from the inhibition of maternal β-catenin. Hence, we performed WISH to examine the expression of the organizer-specific markers *chordin* (*chd*) and *goosecoid* (*gsc*) at 4.3 hpf to assess the development of the dorsal organizer because both markers are main targets of maternal Wnt at this stage. As shown in Fig. 4G and H, embryos injected with *eif4a3* mRNA showed reduced expression areas for *chd* and *gsc*, indicating that Eif4a3 has a ventralizing effect before gastrulation and overexpression of Eif4a3 inhibits maternal Wnt signaling.

We next defined the functional domain(s) of EIF4A3/Eif4a3 involved in ventralizing zebrafish embryos. To this purpose, the mRNAs for various human EIF4A3 mutants (Fig. 2B) were injected into zebrafish embryos to examine the effect on the expression patterns of *chd* and *gsc* at 4.3 hpf and *otx2* at the bud stage. As shown in Fig. S2A-F, EIF4A3ΔD1 mutant completely abolished the ventralizing action, suggesting that DEAD domain 1 of EIF4A3 is required for maternal Wnt inhibiting action. Consistently, zebrafish Eif4a3ΔD1 mutant also lost the inhibitory effect on Wnt3a-induced Wnt reporter activity in zebrafish embryos (Fig. S2G). Thus, we concluded that DEAD domain 1 of EIF4A3/Eif4a3 was required to inhibit Wnt/β-catenin signaling.

The role of EIF4A3/Eif4a3 in RNA processing is ATPase-dependent (Le Hir et al., 2016; Linder and Jankowsky, 2011). To determine whether the function of EIF4A3/Eif4a3 within the RNA processing is required to inhibit Wnt/β-catenin signaling, we generated two mutants of human EIF4A3, K88N and E188Q. Both mutants abolished ATP binding capability according to previously biochemical studies (Gehring et al., 2009; Shibuya et al., 2006). The two mutants exhibited inhibitory effects on the formation of the dorsal organizer at 4.3 hpf (Fig. 4I and J). Overexpression of β-CatΔN strongly induced maternal Wnt activity in zebrafish, leading to expanded expression areas of *chd* and *gsc* at 4.3 hpf (Fig. 4K and L). Like wild-type EIF4A3, both point mutants inhibited the ectopic Wnt activity induced by *β-catΔN* mRNA-injection (Fig. 4K and L). Likewise, in HCT116 cells, EIF4A3 and each point mutant significantly inhibited Wnt reporter activity induced by β-CatΔN (Fig. 4M). The data suggested that overexpression of EIF4A3/Eif4a3 inhibited Wnt/β-catenin signaling and impaired the formation of the dorsal organizer in an RNA processing-independent manner.

Depletion of Eif4a3 impaired dorsoventral pattern formation and anterior neuroectoderm development in zebrafish embryos

The spatiotemporal expression pattern of *eif4a3* in zebrafish embryos suggested that *eif4a3* was maternally deposited and ubiquitously expressed before 24 hpf and then enriched in the head region at 36 hpf and 48 hpf (Fig. S1B, C). The *eif4a3*-null mutant was generated by using the TALEN-based knockout system to explore the physiological role of Eif4a3 (Fig. S3A). We obtained a line with an 8-bp deletion in the third exon of *eif4a3*, which resulted in the early termination of translation (Fig. S3B-D). Western blot analysis showed that Eif4a3 protein levels were gradually reduced in *eif4a3* mutants both at 15 hpf and at 24 hpf (Fig. S3E). We noted that Eif4a3 protein levels were markedly reduced but not completely depleted, suggesting abundant maternally deposited Eif4a3 protein. The zygotic mutant fish exhibited a ventralized phenotype, characterized by a small head, shortened and bent body axes, and a reduced dorsal tail fin, along with apoptotic cells in the whole body at 24 hpf (Fig. S3F-H). These phenotypes could be rescued by the injection of 50 pg of *eif4a3* mRNA (Fig. S3F-G), suggesting that the *eif4a3* knockout is specific.

Increased apoptotic cells and microcephaly were previously observed in mice haploinsufficient for *Eif4a3*, and the genetic ablation of *p53* was sufficient to rescue this phenotype (Mao et al., 2016). Apoptotic cells in *eif4a3*-null mutant embryos may impinge the observation on the effects of Wnt activation. The use of *p53*-null zebrafish could potentially decrease the collateral tissue damage, thus allowing us to observe the important phenotypes masked by p53-induced cell death (Robu et al., 2007). We noted that the ventralized phenotypes by depletion of Eif4a3 retains in *p53* mutant background, other than the lack of apoptotic cells at 24 hpf (Fig. 5A). Additionally, we observed a larger expression domain of *gata1* in the blood island and a smaller expression domain of retina marker *rx1* in the double mutant embryos at 24 hpf (Fig. 5B, C). These results implied that the zebrafish *eif4a3* knockout caused a significant increase in p53-induced apoptosis, which is similar to what occurs in mice; nevertheless, the ventralized phenotype is almost negligible affected by p53-mediated cell apoptosis.

Two non-overlapping translation-blocking morpholinos (MOs) targeting *eif4a3* mRNA were used as an independent and complementary approach to perform *eif4a3* knockdown analysis (Fig. S4A). The MOs effectively blocked the translation of an *eif4a3* 5′-UTR-GFP

reporter (Fig. S4B). Injection of MOs reduced Eif4a3 protein levels in zebrafish embryos at 6 hpf rather than at 4.3 hpf (Fig. S4C). These results suggest that the MOs blocked the translation of *eif4a3* effectively but did not decrease the maternal levels of the Eif4a3 protein. The injection of *eif4a3* MO1 and MO2 resulted in a consistent phenotype at 24 hpf, that of which was similar to those of *eif4a3* mutants (Fig. S4D). This phenotype could also be neutralized by co-injection of 50 pg *eif4a3* mRNA (Fig. S4E). Additionally, ventralized phenotypes were also observed in *eif4a3* morphants with the *p53*$^{-/-}$ genetic background (Fig. S4F). Hereafter, we evaluated effects of depletion of *eif4a3* in zebrafish embryos with the *p53*$^{-/-}$ background.

The above ventralized phenotypes prompted us to investigate whether or not the dorsal organizer formation was impaired after the onset of gastrulation. We, therefore, examined the expression of the dorsoventral marker genes at the shield stage. The *eif4a3*-depleted embryos showed reduced expressions of *chd* and *gsc*, but laterally and dorsally expanded expression of the ventral marker gene *even-skipped-like1* (*eve1*) (Fig. 5D and E, S5A and B). We next investigated anteroposterior neural pattern formation after depletion of *eif4a3*. The expression of *six3b* (the indicative marker of forebrain), *pax2a* (the indicative marker of midbrain-hindbrain boundary), and *krox20* (the indicative marker of hindbrain), were used simultaneously to assess anteroposterior neural patterning. The expression levels of *six3b* and *pax2a* were reduced in *eif4a3* mutants and morphants at 12.5 hpf; however, no apparent alterations in *krox20* levels were observed, suggesting that Eif4a3 promotes anterior neural development (Fig. 5F and S5C). Taken together, these results indicated that the depletion of zygotic Eif4a3 inhibited dorsal and anterior neuroectoderm development. We then investigated the effect of the loss of Eif4a3 on Wnt/β-catenin signals. Knockdown of *eif4a3* significantly increased Wnt reporter activity (Fig. S5D). Additionally, we observed that depletion of Eif4a3 expanded the expression areas of *cdx4* and s*p5l*, two direct target genes of zygotic Wnt, at the 80% epiboly stage, as accessed by WISH (Fig. 5G and Fig. S5E). Similarly, the expression levels of the direct zygotic Wnt targets, *cdx4*, *sp5l*, *vent*, *axin2*, and *ccnd1*, increased in *eif4a3* mutants at the 80% epiboly stage, as indicated by qRT-PCR (Fig. 5H). In addition, EIF4A3 was depleted in HCT116 cells with a *p53*$^{-/-}$ genetic background via a shRNA-mediated knockdown approach (Fig. S5F). Again, the Wnt reporter activity and the transcriptional levels of Wnt target genes were measured. Similarly, knockdown of EIF4A3 in HCT116 cells also increased Wnt reporter activity and transcriptional levels of the direct Wnt target genes, *AXIN2* and *DKK1* (Fig. S5G and H). Therefore, we concluded that depletion of EIF4A3/Eif4a3 increases Wnt/β-catenin signaling in both zebrafish embryos and cultured cells.

Since Bmp, Nodal, and Fgf signaling pathways are also involved in axial patterning in zebrafish (Langdon and Mullins, 2011), it is not clear whether these pathways are affected during gastrulation when Eif4a3 is depleted. Indeed, Bmp, Nodal, and Fgf signaling pathways appear unaffected, as indicated by the expression of a series of marker genes (Fig. S6A-C). Collectively, these data strongly suggest that zebrafish *eif4a3* promotes dorsal development and anterior neuroectoderm pattern formation and depletion of EIF4A3/Eif4a3 increases Wnt/β-catenin signaling.

Tcf7l2 repression counteracts the effects of *eif4a3* depletion in zebrafish embryos

We wondered whether Eif4a3 promotes dorsal development and anterior neuroectoderm pattern formation by inhibiting Wnt/β-catenin signaling. To prove this idea, a Wnt/β-catenin signaling inhibitor, human TCF7L2ΔN, which lacks the β-catenin binding domain and acts as a constitutive repressor of Wnt/β-catenin signaling, was introduced into *eif4a3*-depleted embryos. First, we evaluated the inhibitory effect of TCF7L2ΔN on the increased Wnt activity by depletion of *eif4a3*. Injection of *TCF7L2ΔN* mRNA rendered the expansion of *cdx4* and *sp5l* expression areas in *eif4a3* mutants and morphants at the 80% epiboly stage, suggesting that TCF7L2ΔN antagonizes *eif4a3*-depletion-induced Wnt activity (Fig. 6A and S7A). We then assessed the antagonistic effect of TCF7L2ΔN on dorsoventral and anterior neuroectoderm development in *eif4a3*-depleted embryos. When comparing with *gfp* mRNA-injected *eif4a3* mutants and morphants, injection of *TCF7L2ΔN* mRNA into *eif4a3* mutants and morphants alleviated the *eif4a3*-depletion-induced reduction in *chd* and *gsc*, as well as the expansion of *eve1* at the shield stage (Fig. 6B, C and S7B, C). Notably, when *TCF7L2ΔN* mRNA was injected into *eif4a3* mutants and morphants, a small proportion of embryos exhibited further reduction of expression of *chd* and *gsc* as well as more expanded expression of *eve1* (Fig. 6C and S7C). The tendencies observed here are likely due to the inhibition of maternal Wnt signaling by TCF7L2ΔN.

Previous studies have indicated that hyperactive Wnt signaling leads to the reduction of the anterior neuroectoderm markers, *six3b* and *opl* (Kim et al., 2002; Liu et al., 2013). The well-established zebrafish *apc* mutant exhibited reduced expression domain of the *opl* by constitutively increasing Wnt/β-catenin activity (Liu et al., 2013). We then examined whether Eif4a3 could rescue this effect by acting as a Wnt inhibitor. Consistent with previous report, not only was the ratio of strongly reduced to reduced to normal of *opl* close to 1:2:1, but also the *opl* expression pattern and the embryonic genotypes are correlated very well in the progenies of $apc^{+/-}$ × $apc^{+/-}$ at bud stage (Fig. 6D, E). Injection of *TCF7L2ΔN* mRNA expanded the expression areas of *opl* in embryos with all three genetic backgrounds, in comparison with the *gfp* mRNA-injected group (Fig. 6D, E). Likewise, injection of *eif4a3* mRNA resulted in a similar effect that was observed with *TCF7L2ΔN* mRNA-injected (Fig. 6D, E), albeit the effect of *eif4a3* is not as much as that of *TCF7L2ΔN*. Additionally, we also investigated the reciprocal action between Wnt signaling and Eif4a3 on the development of the anterior neuroectoderm. Introduction of *TCF7L2ΔN* mRNA into *eif4a3*-depleted embryos rescued the expression of *six3b* and *pax2a* at 12.5 hpf (Fig. 6F and Fig. S7D). These results suggest that Eif4a3 promotes dorsal development and anterior neuroectoderm pattern formation by inhibiting Wnt/β-catenin signaling.

Discussion

As a member of the DEAD-box protein family, EIF4A3 is a core component of the EJC. Within the EJC, EIF4A3 exhibits RNA-dependent ATPase activity and ATP-dependent RNA helicase activity. In the present study, we identified a mechanism by which EIF4A3/Eif4a3 suppressed the β-catenin/Tcf transcription complex activity, thereby limiting the output of Wnt signaling. We found that EIF4A3 binds to either β-CATENIN or to TCF7L2 and associates with the promoters of Wnt target genes. EIF4A3 likely competes with β-CATENIN for binding to TCF7L2. EIF4A3 dissociated from a transcriptional complex and promoters of

Wnt target genes with increasing Wnt signaling, suggesting that EIF4A3 acts as a Wnt responsible inhibitor to control β-catenin/Tcf transcriptional activity. In zebrafish embryos, Eif4a3 acts as a Wnt inhibitor to promote dorsal development and anterior neuroectoderm pattern formation.

A key finding of this study is that EIF4A3/Eif4a3 specifically inhibits Wnt/β-catenin signaling. We observed that EIF4A3/Eif4a3 inhibited Wnt activity induced by Wnt3a and β-CatΔN but not by VP16-Tcf7l1ΔN both *in vitro* and *in vivo*. Importantly, injection of *TCF7L2ΔN* rendered the broad expansions of Wnt target genes in *eif4a3*-depleted zebrafish embryos, suggesting that EIF4A3/Eif4a3 acts at the level of β-catenin. Moreover, Wnt reporter activity induced by β-CatΔN/TCF7L2 decreased along with the increasing amounts of EIF4A3. A series of co-IP assays indicated that EIF4A3 associates with β-CATENIN or with TCF7L2 and ChIP assay suggested that EIF4A3 binds to the promoters of Wnt target genes under physiological conditions. When EIF4A3 was overexpressed, the associations of β-CATENIN with TCF7L2 were attenuated as associations of β-CATENIN with EIF4A3 increased in a dose-dependent manner. However, upon Wnt stimulation, the association of EIF4A3 with β-CATENIN and with TCF7L2 decreased as the association of β-CATENIN with TCF7L2 increased, and EIF4A3 was released from the promoter of Wnt target genes. Our results suggested that EIF4A3 and β-CATENIN are mutually exclusive interaction with TCF7L2, and accumulated β-CATENIN would drive TCF7L2 into a complex with β-CATENIN, displacing EIF4A3 by competition with increasing of Wnt stimulation, which leads to release of EIF4A3 from the promoter of Wnt target genes. We do not know where EIF4A3 would go after dissociation from the transcription complex under Wnt stimulation. It has been reported that EIF4A3 can shuttle between the nucleus and cytoplasm (Le Hir et al., 2016). Future studies will be needed to determine the distribution of EIF4A3 responsible for Wnt stimulation. EIF4A3 acts as an inhibitor of Wnt/β-catenin signaling pathway makes a relatively more complicated regulatory mechanism than appears necessary in this pathway. One advantageous possibility is that EIF4A3 likely exists in a pool and disassociates from a transcriptional complex under the stimulation of Wnt signaling to help to shape expression levels of Wnt gradient-induced target genes.

The inhibitory effects of EIF4A3 on the Wnt pathway in cell lines were recapitulated in zebrafish embryos. Eif4a3 regulates dorsoventral pattern formation and anterior neuroectoderm development by inhibiting the Wnt/β-catenin pathway. A previous study indeed showed that misexpression of Eif4a3 inhibited dorsal development of *Xenopus* ectoderm (Weinstein et al., 1997). In zebrafish, overexpression of EIF4A3/Eif4a3 caused ventralized phenotypes at 24 hpf. This ventralizing effect was likely due to the inhibition of maternal Wnt signaling which was supported by the reduced expression of dorsal organizer markers in late blastula stage. Although abundant maternally deposited Eif4a3 mRNA and protein may obscure and alleviate the forced expression effect, we conclude that the ventralizing effect by overexpression of Eif4a3 occurs because maternal Wnt activity is inhibited. Depletion of Eif4a3 by either knockout or knockdown caused a weakly ventralized phenotype and reduced anterior neuroectoderm structure in zebrafish embryos with a $p53^{-/-}$ background. It is conceivable that the contribution of the maternal mRNA and protein may compromise the loss-of-function effect in both zygotic knockout embryos and translation-blocking MO knockdown embryos. In support of this view, the deposited maternal

protein was detected even in zygotic mutant embryos at 24 hpf although we observed a dramatic reduction in the level of Eif4a3 protein from 15 hpf to 24 hpf in *eif4a3* mutant embryos. At first, we expected the translation-blocking MOs to produce dorsalized embryos but we did not observe this. Indeed, the protein levels were reduced at the beginning of gastrulation but were not apparently altered at the late blastula stage, when the knockdown was performed. Therefore, the morphant embryos exhibit a ventralized phenotype similar to that of zygotic mutant embryos due to depletion of the Eif4a3 protein in zygotic Wnt functional stages.

The Wnt/β-catenin signaling pathway plays a key role in anteroposterior neuroectoderm formation in a concentration-dependent manner in multiple animal species (Dorsky et al., 2003; Kiecker and Niehrs, 2001; Rhinn et al., 2005). In zebrafish, overactivation of Wnt signaling leads to neuroectoderm posteriorization (Green et al., 2015; Petersen and Reddien, 2009). We observed that expression levels decreased but the position of the anterior neuroectoderm markers *six3b* and *pax2a* in *eif4a3* mutants and morphants did not shift, whereas the expression pattern of hindbrain marker *krox20* was unchanged. As discussed earlier, our results demonstrate that Eif4a3 inhibits Wnt signaling while the association between Eif4a3 and transcriptional complex becomes attenuated upon Wnt stimulation. Such molecular mechanism implied that Eif4a3 may have inhibitory role with different degree along with the gradient Wnt activity from the anterior to the posterior. This molecular mechanism of Eif4a3 in Wnt signaling suggests that depletion of Eif4a3 resulted in the activity of Wnt increased at different degrees and exhibited distinct action based on the local level of Wnt signaling during anteroposterior neuroectoderm patterning. Zygotic Wnt pathway has relative less activity in anterior comparing with that in posterior. This may explain the anterior neuroectoderm defect in Eif4a3-depleted embryos we observed.

There are two major phenotypes that were observed in zygotic mutant embryos and morphant embryos. First, the depletion of Eif4a3 in zebrafish embryos leads to the apoptotic phenotype while the loss of *p53* significantly rescues this phenotype. Similar effects were observed previously in mice, thus supporting this view. In mice, the conditional haploinsufficiency of *Eif4a3*, *Y14*, or *Magoh* induces apoptosis and p53 ablation rescues apoptosis in the three EJC mutants (Mao et al., 2016). In addition, loss of *Y14* or *Magoh* in zebrafish also leads to the apoptotic phenotype as *Eif4a3* mutant embryos and morphant embryos (Gangras et al., 2020). Therefore, these data suggested that the apoptosis is likely due to the impairment of the EJC complex. Second, zygotic *eif4a3* mutants and *eif4a3* morphants with a $p53^{-/-}$ background exhibited ventralized phenotype and reduced anterior neuroectoderm development with increased Wnt activity. The ventralized phenotype and the reduction in anterior neuroectoderm development are likely due to enhancement of the Wnt/β-catenin signaling pathway. The evidence includes the following two observations: 1) injection of *TCF7L2ΔN* mRNA counteracted the ventralizing effect in Eif4a3-depleted embryos at shield stage; and 2) the genetic interaction between Eif4a3 and the components of the Wnt/β-catenin pathway, Apc and Tcf7l2, occurring in the formation of the anterior neuroectoderm in zebrafish embryos.

It was reported that the EJC complex has various biological functions, and EJC-deficiency triggers p53-induced apoptosis. In *Xenopus*, the depletion of Eif4a3 leads to full-body paralysis by altering the splicing of *ryanodine receptor*, with defects in sensory neurons,

pigment cells, and cardiac development. Similar phenotypes were observed in MOs-mediated knockdown of *magoh* or *Y14* embryos (Haremaki et al., 2010; Haremaki and Weinstein, 2012). Likewise, the conditional haploinsufficiency of *Eif4a3*, *Y14*, and *Magoh* in mice results in highly similar embryonic neurogenesis defect and microcephaly as does activation of p53. Furthermore, the genetic ablation of *p53* significantly rescues microcephaly in mice with the conditional haploinsufficiency of all three EJC subunits (Mao et al., 2016; Mao et al., 2015; McMahon et al., 2014; Silver et al., 2010). In *Drosophila*, Eif4a3, Magoh, and Y14 maintained *MAPK* transcript levels, and depletion of Eif4a3, Magoh, or Y14 led to photoreceptor differentiation defects and extensive apoptosis (Roignant and Treisman, 2010). Intriguingly, the depletion of Eif4a3, Magoh, or Y14 in *Drosophila* results in phenotypes associated with reduced Wnt signaling, suggesting that EJC positively regulates the Wnt/β-catenin signaling pathway. Mechanistically, the EJC controls the splicing of *dlg1*, and Dlg1 interacts directly with Dsh to protect it from lysosomal degradation (Liu et al., 2016). Overall, the effects of Eif4a3 observed in various organisms can likely be explained by its function as a core subunit within the EJC, since the depletion of other EJC subunits result in similar effects. These phenotypes are different than those observed in zebrafish *eif4a3* mutants. Considering the broad role of the EJCs in posttranscriptional processes, it is possible that the depletion of *eif4a3* impedes other pathways directly or indirectly and this may contribute to this observation. However, our data demonstrated that Bmp, Nodal, and Fgf signaling pathways, which are all involved in axial patterning, are not affected by the depletion of Eif4a3 in zebrafish embryos during gastrulation.

In humans, the biallelic expansion of a complex repeat motif in the 5' untranslated region of *EIF4A3* reduces the level of *EIF4A3* transcript and causes RCPS, which is mainly characterized by craniofacial and limb malformations (Favaro et al., 2014; Favaro et al., 2011; Hsia et al., 2018). Alterations in the physiological functions of EIF4A3 might contribute to RCPS (Mao et al., 2016). Wnt/β-catenin signaling plays important roles in cranial skeletogenesis and limb formation (Delgado and Torres, 2017; Regard et al., 2012). For example, the genetic ablation of the Wnt inhibitors, *Axin2* and *Nkd1/2*, in mice alters cranial bone morphology (Liu et al., 2007; Yu et al., 2005; Zhang et al., 2007). Our study reveals that EIF4A3 functions as an inhibitor of canonical Wnt signaling. These findings improve our understanding of the molecular mechanisms underlying EIF4A3/Eif4a3 function at the cellular level and during embryonic development. Future studies of EIF4A3 as a Wnt modifier will shed light on the specificity of the molecular regulation of Wnt pathway and may contribute to understand the mechanisms of RCPS.

Materials and Methods

Chemicals, reagents, and antibodies

Restriction enzymes were purchased from New England BioLabs (Ipswich, MA, USA). Oligo$(dT)_{18}$ was purchased from Sangon Biotech (Shanghai, China). DIG-UTP and anti-digoxigenin-AP were purchased from Roche (Indianapolis, IN, USA). M-MLV Reverse Transcriptase and the Dual-Glo Luciferase Assay System were purchased from Promega (Madison, WI, USA). The mMESSAGE mMACHINE mRNA Synthesis Kit was purchased from Ambion (Austin, TX, USA). KOD DNA polymerase was purchased from Toyobo (Osaka, Japan). Dulbecco's Modified Eagle's Medium (DMEM) was purchased from Hyclone (Logan, UT, USA). Fetal bovine serum (FBS) was purchased from PAN (Aidenbach,

Germany). Morpholino oligonucleotides were purchased from Gene Tools, LLC (Philomath, OR, USA). Protein A/G Plus-agarose was purchased from Santa Cruz Biotechnology (Santa Cruz, CA, USA). The following antibodies were used in this study: mouse anti-EIF4A3 (1:1000 for western blotting, 1:200 for immunocytochemistry, 2 μg for co-IP and ChIP assays, 05-1527; Millipore, Burlington, MA, USA), rabbit anti-EIF4A3 (1:1000 for western blotting, sc-67369; Santa Cruz, CA, USA), rabbit anti-EIF4A3 (1:1000 for western blotting, ab32485; Abcam, Cambridge, UK), rabbit anti-TCF7L2 (1:1000 for western blotting and 2 μg for co-IP assays, #2569; Cell Signaling, Danvers, MA, USA), mouse anti-β-catenin (1:1000 for western blotting and 2 μg for co-IP assays, M24002; Abmart, Shanghai, China), rabbit anti-non-phospho-β-catenin (1:1000 for western blotting, #8814; Cell Signaling), rabbit anti-GAPDH (1:1000 for western blotting, D110016; BBI, Crumlin, UK), mouse anti-Myc (1:1000 for western blotting and 2 μg for co-IP assays, sc-40; Santa Cruz), murine anti-Flag (1:1000 for western blotting and 2 μg for co-IP assays, F1804; Sigma, St. Louis, MO, USA), rabbit anti-HA (1:1000 for western blotting and 2 μg for co-IP assays, #3724; Cell Signaling, Danvers, MA, USA), and rabbit anti-Histone H3 (1:1000 for western blotting, P30266M; Abmart, Shanghai, China).

Zebrafish strains

The wild-type zebrafish (*Danio rerio*) strain Tübingen and *p53*-defective mutant strain *tp53*^{M214K} were maintained on a 14h light/10h dark cycle at 28.5°C and fed twice daily. The *eif4a3*-knockout mutant strain was constructed using the TALEN system. The *eif4a3* and *p53* double mutant strain was obtained by natural crossing. Embryos obtained by natural crosses were kept in embryo rearing solution in an incubator at 28.5°C. Embryos were strictly staged according to standard methods (Kimmel et al., 1995).

Ethics statement

All experimental protocols were approved by and conducted in accordance with the Ethical Committee of Experimental Animal Care, Ocean University of China.

Molecular cloning and plasmid construction

The sequences of human *EIF4A3* and zebrafish *eif4a3* were retrieved from NCBI (GenBank accession number: NC_000017.11 and NC_007122.7). The full-length cDNA of zebrafish *eif4a3* and human *EIF4A3* with/without the 3'-UTR were amplified and cloned into the pCS2+ expression vector. EIF4A3 domain-deleted mutant sequences (domain 1, domain 2, C-terminus, N-terminus, and the middle section were deleted) were amplified and subcloned into the pCS2+ expression vector. All primers used in this study are listed in supplementary table 1. The amino acid sequence alignment was performed using ClustalX and GeneDoc.

RT-PCR, whole-mount *in situ* hybridization, and acridine orange (AO) staining

Total RNA was isolated from zebrafish embryos using TRIzol reagent (Invitrogen, Carlsbad, CA, USA). The cDNAs were reverse-transcribed using Oligo(dT)$_{18}$ and M-MLV into first-strand cDNA according to the manufacturer's instructions. RT-PCR was performed using Taq DNA polymerase. Quantitative real-time RT-PCR (qRT-PCR) was performed using an iCycler iQ Multicolor Real-time PCR Detection System (Bio-Rad Laboratories, Hercules, CA, USA). Samples from three independent experiments were collected and each sample was measured in duplicate. The mRNA levels of the genes of interest were calculated using the $2^{-\Delta\Delta Ct}$ method and normalized to *β-actin* or *GAPDH*.

Whole-mount *in situ* hybridization using a DIG-labeled RNA riboprobe was performed as previously described (Feng et al., 2012; Rong et al., 2014; Rong et al., 2017). The plasmid DNA containing partial ORF and the 3′ untranslated region (UTR) from zebrafish *eif4a3* was used to generate sense and antisense riboprobes. The specificity of the riboprobes was verified by a dot-blot analysis. Images were obtained using a dissecting stereo microscope.

For detecting the apoptotic cells, AO (Sigma A1121) staining was performed as previously described (Liu et al., 2014).

Capped mRNA synthesis, morpholinos, and microinjection

Capped mRNA was synthesized using the mMESSAGE mMACHINE Kit. To knock down *eif4a3*, two translation-blocking morpholino oligonucleotides (MOs) targeting *eif4a3* were designed and purchased from Gene Tools according the targeting guideline (Philomath, OR, USA). The sequences of MOs are listed in supplementary figure S4A. A standard control MO (5′-CCTCTTACCTCAGTTACAATTTATA-3′) from Gene Tools was used as the control. A GFP reporter plasmid containing the 5′-UTR and partial ORF (-106–564 bp) of zebrafish *eif4a3* was constructed and used to examine the efficiency of the MOs. All MOs were diluted to the desired concentration. Diluted MO and/or mRNA were injected into one-cell stage zebrafish embryos. After injection, the embryos were placed in embryo-rearing medium and maintained at 28.5°C.

Cell culture and luciferase assays

HEK293T and HCT116 cells were purchased from the ATCC (Manassas, VA, USA). Cells were cultured in DMEM medium with 10% FBS and 1% PS (penicillin and streptomycin) in a humid 37°C incubator containing 5% CO_2.

Cells were seeded into 12-well plates to reach 70%-80% confluence at the time of transfection. Transfections were performed in dishes by using Polyethylenimine (Polysciences, cat# 23966-2). Plasmids were co-transfected with 240 ng of TOPFlash DNA and 40 ng of *Renilla* DNA. The empty pCS2+ vector was used both as a control and to adjust the DNA amount to 1.0-1.5 μg/well. After 24 h, a luciferase reporter assay was performed using a Dual-Luciferase Assay Kit. TOPFlash luciferase activity was normalized by the luciferase activity of *Renilla*. The *in vivo* luciferase assay was performed as previously described (Feng et al., 2012; Rong et al., 2014; Rong et al., 2017). Briefly, one- to two-cell stage embryos were injected with MOs and/or mRNA plus 100 pg of TOPFlash DNA and 20 pg of *Renilla* plasmid DNA and then reared to the shield stage. Two independent groups of embryos (each with more than 20 embryos) were lysed and measured each time.

Stable EIF4A3 knockdown cell line construction

The stable EIF4A3 knockdown cell line was established by lentiviral delivery of shRNA in the HCT116 cell line with a $p53^{-/-}$ genetic background (a gift from Dr. Jun Chen). EIF4A3 shRNA-1 sequence 5’-GGATATTCAGGTTCGTGAA-3’ and EIF4A3 shRNA-2 sequence 5’-GCTCTCGGTGACTACATGA-3’ were used (Alexandrov et al., 2011). The lentiviral pLKO.1-GFP + Puromycin vector was selected as a shuttle vector. The shEIF4A3 plasmid and two packaging plasmids were co-transfected into HEK293T cells. After 48 h, supernatant was collected and filtered through a 0.22 μm filter. Viral supernatant containing 8 μg/mL polybrene was added to 30–40% confluent HCT116 cells for infection. After 48 h of incubation, the puromycin was added to select puromycin-resistant cells. The knockdown efficiency was detected by immunoblotting.

Immunoprecipitation and immunoblotting

Cells were transfected with various constructs at 70%-80% confluence and harvested 24 h after transfection. Protein complexes were precipitated from whole-cell lysate or indicated zebrafish embryos deyolk lysates with indicated IP antibodies and enriched by protein A/G PLUS-Agarose. Immunoprecipitates were eluted by boiling the beads in loading buffer, followed by immunoblotting.

Cell lysates, embryonic extracts, or immunoprecipitated protein eluates were separated by SDS-PAGE and blotted onto PVDF membranes for immunoblotting. GAPDH and Histone H3 were detected as the loading control when needed. All results are from three independent experiments. The figures shown are representative results.

Immunocytochemistry

HeLa cells were fixed with 4% paraformaldehyde for 10 min at room temperature, followed by 0.2% Triton X-100 treatment for 5 min and blocking with 20% BSA (Bull Serum Albumin). The cells were then incubated with corresponding primary and secondary antibodies along with DAPI for visualization of the nuclei. Fluorescence images were acquired with a Leica TCS SP8 confocal microscope.

GST-pulldown assay

Expression of GST or GST-tagged EIF4A3 in *E. coli* BL21(DE3) cells was induced using 0.1 mM IPTG; cells were allowed to grow for 2 h at 37℃. GST fusion proteins were affinity-purified on a glutathione Sepharose 4B (GE Healthcare) according to the manufacturer's instructions. Then, HEK293T cells were transfected with Flag-tagged β-CATENIN or Myc-tagged TCF7L2. These proteins of cell lysates were incubated with GST or GST-tagged EIF4A3 with continuous rotation at 4°C for overnight. Proteins were washed 4 times to remove non-specific bound proteins from the bead. After incubation, proteins bound to the agarose beads were eluted in SDS sample buffer by boiling and analyzed by standard western blotting.

ChIP assay

ChIP assays were conducted using a ChIP Assay Kit (Millipore) according to the manufacturer's protocol. Briefly, HEK293T cells (2×10^7) were fixed with fresh formaldehyde. Chromatin in cell lysates was sheered to ~300–900 base pairs in length using a VCX 130 Sonicator (Sonics & Materials, Inc., Newtown, CA, USA; 18 × 10-s on, 17 × 10-s pulses, 30% amplitude, ChIP samples kept on ice water). Precipitated DNA samples were analyzed by semi-quantitative and quantitative PCR. The qPCR data were expressed as the percentage of input DNA. Samples from three independent experiments were used and each sample was measured in duplicate. The representative figures of semi-quantitative PCR are shown.

Statistical analysis

Data are presented as means ± S.E.M. Student's *t*-tests were used for comparisons between two groups or one-way analysis of variance followed by Tukey's post test were used for comparisons among multiple groups. Differences among groups were analyzed using GraphPad Prism version 5.01 (San Diego, CA, USA) and significance was defined as $p < 0.05$ or smaller p values.

Acknowledgements

We are grateful to Dr. Cunming Duan from University of Michigan, Ann Arbor for critical suggestions. We thank for Dr. Hongyan Li from Ocean University of China for helping to generate plasmids of TALENs, Dr. Anming Meng from Tsinghua University, Dr. Jun Chen from Zhejiang University, Dr. Ying Cao from Nanjing University, and Dr. Ming Shao from Shandong University for providing reagents.

Financial disclosure

This work was supported by the National Key R & D Program of China (2018YFA0801000 to JZ), the National Natural Science Foundation of China-Shandong Joint Fund (U1606403 to JZ), the Fundamental Research Funds for the Central Universities (201822023 to JZ, 201762022 to XR), the National Natural Science Foundation of China (31601863 to XR, 31872189 to JZ, and 30972238 to JZ), and the Natural Science Foundation of Shandong Province (ZR2017MC001 to JZ). The funders had no role in study design, data collection and analysis, decision to publish, or preparation of the manuscript.

References

Alexandrov, A., Colognori, D. and Steitz, J. A. (2011). Human eIF4AIII interacts with an eIF4G-like partner, NOM1, revealing an evolutionarily conserved function outside the exon junction complex. *Genes & development* **25**, 1078-1090.

Ashton-Beaucage, D., Udell, C. M., Lavoie, H., Baril, C., Lefrancois, M., Chagnon, P., Gendron, P., Caron-Lizotte, O., Bonneil, E., Thibault, P., et al. (2010). The exon junction complex controls the splicing of MAPK and other long intron-containing transcripts in Drosophila. *Cell* **143**, 251-262.

Baker, K. D., Ramel, M. C. and Lekven, A. C. (2010). A direct role for Wnt8 in ventrolateral mesoderm patterning. *Developmental dynamics : an official publication of the American Association of Anatomists* **239**, 2828-2836.

Bellipanni, G., Varga, M., Maegawa, S., Imai, Y., Kelly, C., Myers, A. P., Chu, F., Talbot, W. S. and Weinberg, E. S. (2006). Essential and opposing roles of zebrafish beta-catenins in the formation of dorsal axial structures and neurectoderm. *Development* **133**, 1299-1309.

Chazal, P. E., Daguenet, E., Wendling, C., Ulryck, N., Tomasetto, C., Sargueil, B. and Le Hir, H. (2013). EJC core component MLN51 interacts with eIF3 and activates translation. *Proceedings of the National Academy of Sciences of the United States of America* **110**, 5903-5908.

Choi, S. H., Estaras, C., Moresco, J. J., Yates, J. R., 3rd and Jones, K. A. (2013). alpha-Catenin interacts with APC to regulate beta-catenin proteolysis and transcriptional repression of Wnt target genes. *Genes & development* **27**, 2473-2488.

Clevers, H. and Nusse, R. (2012). Wnt/beta-catenin signaling and disease. *Cell* **149**, 1192-1205.

Delgado, I. and Torres, M. (2017). Coordination of limb development by crosstalk among axial patterning pathways. *Developmental biology* **429**, 382-386.

Dorsky, R. I., Itoh, M., Moon, R. T. and Chitnis, A. (2003). Two tcf3 genes cooperate to pattern the zebrafish brain. *Development* **130**, 1937-1947.

Erter, C. E., Wilm, T. P., Basler, N., Wright, C. V. and Solnica-Krezel, L. (2001). Wnt8 is required in lateral mesendodermal precursors for neural posteriorization in vivo. *Development* **128**, 3571-3583.

Favaro, F. P., Alvizi, L., Zechi-Ceide, R. M., Bertola, D., Felix, T. M., de Souza, J., Raskin, S., Twigg, S. R., Weiner, A. M., Armas, P., et al. (2014). A noncoding expansion in EIF4A3 causes Richieri-Costa-Pereira syndrome, a craniofacial disorder associated with limb defects. *American journal of human genetics* **94**, 120-128.

Favaro, F. P., Zechi-Ceide, R. M., Alvarez, C. W., Maximino, L. P., Antunes, L. F., Richieri-Costa, A. and Guion-Almeida, M. L. (2011). Richieri-Costa-Pereira syndrome: a unique acrofacial dysostosis type. An overview of the Brazilian cases. *Am J Med Genet A* **155A**, 322-331.

Feng, Q., Zou, X., Lu, L., Li, Y., Liu, Y., Zhou, J. and Duan, C. (2012). The stress-response gene redd1 regulates dorsoventral patterning by antagonizing Wnt/beta-catenin activity in zebrafish. *PloS one* **7**, e52674.

Gangras, P., Gallagher, T. L., Parthun, M. A., Yi, Z., Patton, R. D., Tietz, K. T., Deans, N. C., Bundschuh, R., Amacher, S. L. and Singh, G. (2020). Zebrafish rbm8a and magoh mutants reveal EJC developmental functions and new 3'UTR intron-containing NMD targets. *PLoS genetics* **16**, e1008830.

Gehring, N. H., Kunz, J. B., Neu-Yilik, G., Breit, S., Viegas, M. H., Hentze, M. W. and Kulozik, A. E. (2005). Exon-junction complex components specify distinct routes of nonsense-mediated mRNA decay with differential cofactor requirements. *Molecular cell* **20**, 65-75.

Gehring, N. H., Lamprinaki, S., Hentze, M. W. and Kulozik, A. E. (2009). The hierarchy of exon-junction complex assembly by the spliceosome explains key features of mammalian nonsense-mediated mRNA decay. *PLoS biology* **7**, e1000120.

Green, D., Whitener, A. E., Mohanty, S. and Lekven, A. C. (2015). Vertebrate nervous system posteriorization: Grading the function of Wnt signaling. *Developmental dynamics : an official publication of the American Association of Anatomists* **244**, 507-512.

Hachet, O. and Ephrussi, A. (2004). Splicing of oskar RNA in the nucleus is coupled to its cytoplasmic localization. *Nature* **428**, 959-963.

Haremaki, T., Sridharan, J., Dvora, S. and Weinstein, D. C. (2010). Regulation of vertebrate embryogenesis by the exon junction complex core component Eif4a3. *Developmental dynamics : an official publication of the American Association of Anatomists* **239**, 1977-1987.

Haremaki, T. and Weinstein, D. C. (2012). Eif4a3 is required for accurate splicing of the Xenopus laevis ryanodine receptor pre-mRNA. *Developmental biology* **372**, 103-110.

Hikasa, H. and Sokol, S. Y. (2013). Wnt signaling in vertebrate axis specification. *Cold Spring Harbor perspectives in biology* **5**, a007955.

Hsia, G. S. P., Musso, C. M., Alvizi, L., Brito, L. A., Kobayashi, G. S., Pavanello, R. C. M., Zatz, M., Gardham, A., Wakeling, E., Zechi-Ceide, R. M., et al. (2018). Complexity of the 5' Untranslated Region of EIF4A3, a Critical Factor for Craniofacial and Neural Development. *Front Genet* **9**, 149.

Kiecker, C. and Niehrs, C. (2001). A morphogen gradient of Wnt/beta-catenin signalling regulates anteroposterior neural patterning in Xenopus. *Development* **128**, 4189-4201.

Kim, S. H., Shin, J., Park, H. C., Yeo, S. Y., Hong, S. K., Han, S., Rhee, M., Kim, C. H., Chitnis, A. B. and Huh, T. L. (2002). Specification of an anterior neuroectoderm patterning by Frizzled8a-mediated Wnt8b signalling during late gastrulation in zebrafish. *Development* **129**, 4443-4455.

Kimmel, C. B., Ballard, W. W., Kimmel, S. R., Ullmann, B. and Schilling, T. F. (1995). Stages of embryonic development of the zebrafish. *Developmental dynamics : an official publication of the American Association of Anatomists* **203**, 253-310.

Langdon, Y. G. and Mullins, M. C. (2011). Maternal and zygotic control of zebrafish dorsoventral axial patterning. *Annual review of genetics* **45**, 357-377.

Le Hir, H., Gatfield, D., Izaurralde, E. and Moore, M. J. (2001). The exon-exon junction complex provides a binding platform for factors involved in mRNA export and nonsense-mediated mRNA decay. *The EMBO journal* **20**, 4987-4997.

Le Hir, H., Sauliere, J. and Wang, Z. (2016). The exon junction complex as a node of post-transcriptional networks. *Nature reviews. Molecular cell biology* **17**, 41-54.

Lekven, A. C., Thorpe, C. J., Waxman, J. S. and Moon, R. T. (2001). Zebrafish wnt8 encodes two wnt8 proteins on a bicistronic transcript and is required for mesoderm and neurectoderm patterning. *Developmental cell* **1**, 103-114.

Linder, P. and Jankowsky, E. (2011). From unwinding to clamping - the DEAD box RNA helicase family. *Nature reviews. Molecular cell biology* **12**, 505-516.

Liu, B., Yu, H. M. and Hsu, W. (2007). Craniosynostosis caused by Axin2 deficiency is mediated through distinct functions of beta-catenin in proliferation and differentiation. *Developmental biology* **301**, 298-308.

Liu, C., Luan, J., Bai, Y., Li, Y., Lu, L., Liu, Y., Hakuno, F., Takahashi, S., Duan, C. and Zhou, J. (2014). Aspp2 negatively regulates body growth but not developmental timing by modulating IRS signaling in zebrafish embryos. *Gen Comp Endocrinol* **197**, 82-91.

Liu, J. X., Zhang, D., Xie, X., Ouyang, G., Liu, X., Sun, Y. and Xiao, W. (2013). Eaf1 and Eaf2 negatively regulate canonical Wnt/beta-catenin signaling. *Development* **140**, 1067-1078.

Liu, M., Li, Y., Liu, A., Li, R., Su, Y., Du, J., Li, C. and Zhu, A. J. (2016). The exon junction complex regulates the splicing of cell polarity gene dlg1 to control Wingless signaling in development. *eLife* **5**.

Lu, L., Gao, Y., Zhang, Z., Cao, Q., Zhang, X., Zou, J. and Cao, Y. (2015). Kdm2a/b Lysine Demethylases Regulate Canonical Wnt Signaling by Modulating the Stability of Nuclear beta-Catenin. *Developmental cell* **33**, 660-674.

MacDonald, B. T. and He, X. (2012). Frizzled and LRP5/6 receptors for Wnt/beta-catenin signaling. *Cold Spring Harbor perspectives in biology* **4**.

MacDonald, B. T., Tamai, K. and He, X. (2009). Wnt/beta-catenin signaling: components, mechanisms, and diseases. *Developmental cell* **17**, 9-26.

Mao, H., McMahon, J. J., Tsai, Y. H., Wang, Z. and Silver, D. L. (2016). Haploinsufficiency for Core Exon Junction Complex Components Disrupts Embryonic Neurogenesis and Causes p53-Mediated Microcephaly. *PLoS genetics* **12**, e1006282.

Mao, H., Pilaz, L. J., McMahon, J. J., Golzio, C., Wu, D., Shi, L., Katsanis, N. and Silver, D. L. (2015). Rbm8a haploinsufficiency disrupts embryonic cortical development resulting in microcephaly. *The Journal of neuroscience : the official journal of the Society for Neuroscience* **35**, 7003-7018.

McMahon, J. J., Shi, L. and Silver, D. L. (2014). Generation of a Magoh conditional allele in mice. *Genesis* **52**, 752-758.

Michelle, L., Cloutier, A., Toutant, J., Shkreta, L., Thibault, P., Durand, M., Garneau, D., Gendron, D., Lapointe, E., Couture, S., et al. (2012). Proteins associated with the exon junction complex also control the alternative splicing of apoptotic regulators. *Molecular and cellular biology* **32**, 954-967.

Miller, E. E., Kobayashi, G. S., Musso, C. M., Allen, M., Ishiy, F. A. A., de Caires, L. C., Jr., Goulart, E., Griesi-Oliveira, K., Zechi-Ceide, R. M., Richieri-Costa, A., et al. (2017). EIF4A3 deficient human iPSCs and mouse models demonstrate neural crest defects that underlie Richieri-Costa-Pereira syndrome. *Human molecular genetics* **26**, 2177-2191.

Mohr, S. E., Dillon, S. T. and Boswell, R. E. (2001). The RNA-binding protein Tsunagi interacts with Mago Nashi to establish polarity and localize oskar mRNA during Drosophila oogenesis. *Genes & development* **15**, 2886-2899.

Newmark, P. A. and Boswell, R. E. (1994). The mago nashi locus encodes an essential product required for germ plasm assembly in Drosophila. *Development* **120**, 1303-1313.

Niehrs, C. (2012). The complex world of WNT receptor signalling. *Nature reviews. Molecular cell biology* **13**, 767-779.

Nott, A., Le Hir, H. and Moore, M. J. (2004). Splicing enhances translation in mammalian cells: an additional function of the exon junction complex. *Genes & development* **18**, 210-222.

Nusse, R. and Clevers, H. (2017). Wnt/beta-Catenin Signaling, Disease, and Emerging Therapeutic Modalities. *Cell* **169**, 985-999.

Palacios, I. M., Gatfield, D., St Johnston, D. and Izaurralde, E. (2004). An eIF4AIII-containing complex required for mRNA localization and nonsense-mediated mRNA decay. *Nature* **427**, 753-757.

Petersen, C. P. and Reddien, P. W. (2009). Wnt signaling and the polarity of the primary body axis. *Cell* **139**, 1056-1068.

Polakis, P. (2012). Drugging Wnt signalling in cancer. *The EMBO journal* **31**, 2737-2746.

Ramel, M. C., Buckles, G. R., Baker, K. D. and Lekven, A. C. (2005). WNT8 and BMP2B co-regulate non-axial mesoderm patterning during zebrafish gastrulation. *Developmental biology* **287**, 237-248.

Regard, J. B., Zhong, Z., Williams, B. O. and Yang, Y. (2012). Wnt signaling in bone development and disease: making stronger bone with Wnts. *Cold Spring Harbor perspectives in biology* **4**.

Rhinn, M., Lun, K., Luz, M., Werner, M. and Brand, M. (2005). Positioning of the midbrain-hindbrain boundary organizer through global posteriorization of the neuroectoderm mediated by Wnt8 signaling. *Development* **132**, 1261-1272.

Robu, M. E., Larson, J. D., Nasevicius, A., Beiraghi, S., Brenner, C., Farber, S. A. and Ekker, S. C. (2007). p53 activation by knockdown technologies. *PLoS genetics* **3**, e78.

Roignant, J. Y. and Treisman, J. E. (2010). Exon junction complex subunits are required to splice Drosophila MAP kinase, a large heterochromatic gene. *Cell* **143**, 238-250.

Rong, X., Chen, C., Zhou, P., Zhou, Y., Li, Y., Lu, L., Liu, Y., Zhou, J. and Duan, C. (2014). R-spondin 3 regulates dorsoventral and anteroposterior patterning by antagonizing Wnt/beta-catenin signaling in zebrafish embryos. *PloS one* **9**, e99514.

Rong, X., Zhou, Y., Liu, Y., Zhao, B., Wang, B., Wang, C., Gong, X., Tang, P., Lu, L., Li, Y., et al. (2017). Glutathione peroxidase 4 inhibits Wnt/beta-catenin signaling and regulates dorsal organizer formation in zebrafish embryos. *Development* **144**, 1687-1697.

Sato, N., Meijer, L., Skaltsounis, L., Greengard, P. and Brivanlou, A. H. (2004). Maintenance of pluripotency in human and mouse embryonic stem cells through activation of Wnt signaling by a pharmacological GSK-3-specific inhibitor. *Nat Med* **10**, 55-63.

Shibuya, T., Tange, T. O., Stroupe, M. E. and Moore, M. J. (2006). Mutational analysis of human eIF4AIII identifies regions necessary for exon junction complex formation and nonsense-mediated mRNA decay. *Rna* **12**, 360-374.

Silver, D. L., Watkins-Chow, D. E., Schreck, K. C., Pierfelice, T. J., Larson, D. M., Burnetti, A. J., Liaw, H. J., Myung, K., Walsh, C. A., Gaiano, N., et al. (2010). The exon junction complex component Magoh controls brain size by regulating neural stem cell division. *Nature neuroscience* **13**, 551-558.

Valenta, T., Hausmann, G. and Basler, K. (2012). The many faces and functions of beta-catenin. *The EMBO journal* **31**, 2714-2736.

van Eeden, F. J., Palacios, I. M., Petronczki, M., Weston, M. J. and St Johnston, D. (2001). Barentsz is essential for the posterior localization of oskar mRNA and colocalizes with it to the posterior pole. *The Journal of cell biology* **154**, 511-523.

Weinstein, D. C., Honore, E. and Hemmati-Brivanlou, A. (1997). Epidermal induction and inhibition of neural fate by translation initiation factor 4AIII. *Development* **124**, 4235-4242.

Wu, B., Piloto, S., Zeng, W., Hoverter, N. P., Schilling, T. F. and Waterman, M. L. (2013). Ring Finger Protein 14 is a new regulator of TCF/beta-catenin-mediated transcription and colon cancer cell survival. *EMBO reports* **14**, 347-355.

Yan, L., Chen, J., Zhu, X., Sun, J., Wu, X., Shen, W., Zhang, W., Tao, Q. and Meng, A. (2018). Maternal Huluwa dictates the embryonic body axis through beta-catenin in vertebrates. *Science* **362**.

Yu, H. M., Jerchow, B., Sheu, T. J., Liu, B., Costantini, F., Puzas, J. E., Birchmeier, W. and Hsu, W. (2005). The role of Axin2 in calvarial morphogenesis and craniosynostosis. *Development* **132**, 1995-2005.

Zhang, S., Cagatay, T., Amanai, M., Zhang, M., Kline, J., Castrillon, D. H., Ashfaq, R., Oz, O. K. and Wharton, K. A., Jr. (2007). Viable mice with compound mutations in the Wnt/Dvl pathway antagonists nkd1 and nkd2. *Molecular and cellular biology* **27**, 4454-4464.

Figures

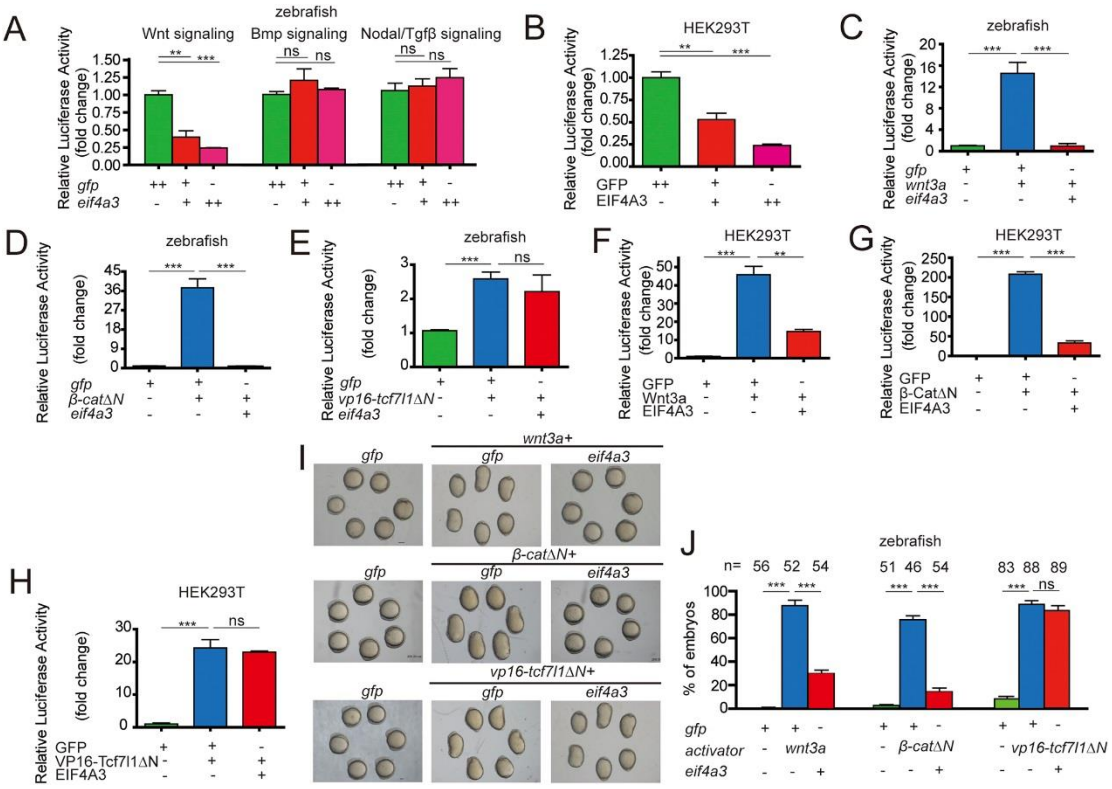

Fig. 1 EIF4A3/Eif4a3 inhibits Wnt/β-catenin signaling at the β-catenin level. (A, B) Overexpression of EIF4A3/Eif4a3 inhibits endogenous Wnt reporter activity *in vivo* and *in vitro*. (A) Embryos were injected with TOPFlash reporter (Wnt/β-catenin signaling) DNA, BRE reporter (Bmp signaling) DNA, or ARE reporter (Nodal/Tgfβ signaling) DNA with 800 pg and 1200 pg of either *gfp* or *eif4a3* mRNA, and luciferase activity was measured at 6 hpf. (B) HEK293T cells were transfected with 800 ng and 1200 ng of GFP plasmid DNA or EIF4A3 plasmid DNA together with TOPFlash reporter DNA, and luciferase activity was measured. (C-E) Eif4a3 inhibits Wnt activity induced by Wnt3a and β-CatΔN, but not by VP16-Tcf7l1ΔN *in vivo*. Embryos were injected with TOPFlash reporter DNA with the indicated mRNAs (200 pg of *wnt3a*, 60 pg of *β-catΔN*, or 200 pg of *vp16-tcf7l1ΔN*) plus 800 pg of *eif4a3* mRNA. (F-H) EIF4A3 inhibits Wnt activity induced by Wnt3a and β-CatΔN, but not by VP16-Tcf7l1ΔN *in vitro*. HEK293T cells were transfected with TOPFlash reporter DNA with the plasmids of the indicated Wnt activator (20 ng of Wnt3a, 30 ng of β-CatΔN, or 200 ng of VP16-Tcf7l1ΔN) plus 800 ng of EIF4A3 plasmid. (I, J) Eif4a3 inhibits the action of indicated Wnt activators *in vivo*. Representative images of embryos injected with 850 pg of *gfp*, mRNA of each indicated Wnt activator (20 pg of *wnt3a*, 50 pg of *β-catΔN*, or 100 pg of *vp16-tcf7l1ΔN*), and mRNA of each activator plus 800 pg of *eif4a3* mRNA at 12.5 hpf are shown in I. Quantitative results are shown in J. The results are from three independent experiments and the total embryo number is given at the top. Values are means ± S.E.M. (n = 3). $^{**}p < 0.01$; $^{***}p < 0.001$; ns, not significant. Unpaired *t*-test, two-tailed. Scale bars: 200 μm.

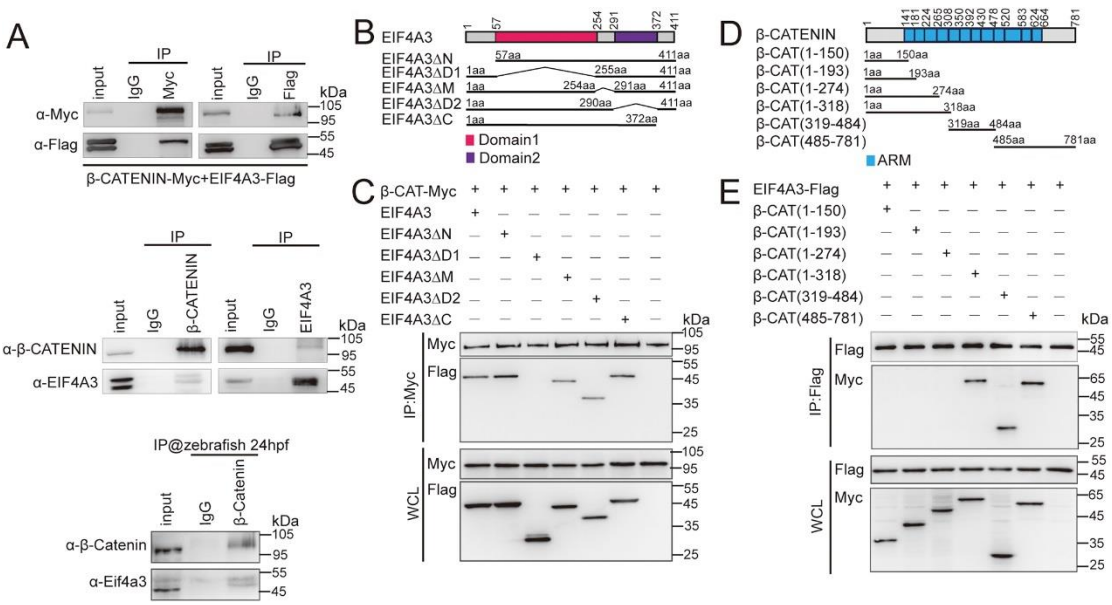

Fig. 2 EIF4A3/Eif4a3 associates with β-CATENIN/β-catenin. (A) EIF4A3/Eif4a3 interacts with β-CATENIN/β-catenin as indicated by co-immunoprecipitation. Upper panel: Exogenous EIF4A3 interacts with β-CATENIN. Middle panel: Endogenous β-CATENIN and EIF4A3 interacted with each other in HEK293T cells. Lower panel: Endogenous β-Catenin and Eif4a3 interacted with each other in zebrafish embryos at 24 hpf. (B, C) Determination of the region of EIF4A3 required for the interaction with β-CATENIN. Schematic diagram of human EIF4A3 protein domains were shown in (B). Various Flag-tagged EIF4A3 mutants were co-expressed with Myc-tagged β-CATENIN in HEK293T cells and cell lysates were subjected to co-immunoprecipitation (C). (D, E) Determination of the region of β-CATENIN required for the EIF4A3 interaction. Schematic diagram of human β-CATENIN protein domains was shown in (D). Various Myc-tagged β-CATENIN truncations were co-expressed with Flag-tagged EIF4A3 in HEK293T cells and cell lysates were subjected to co-immunoprecipitation (E).

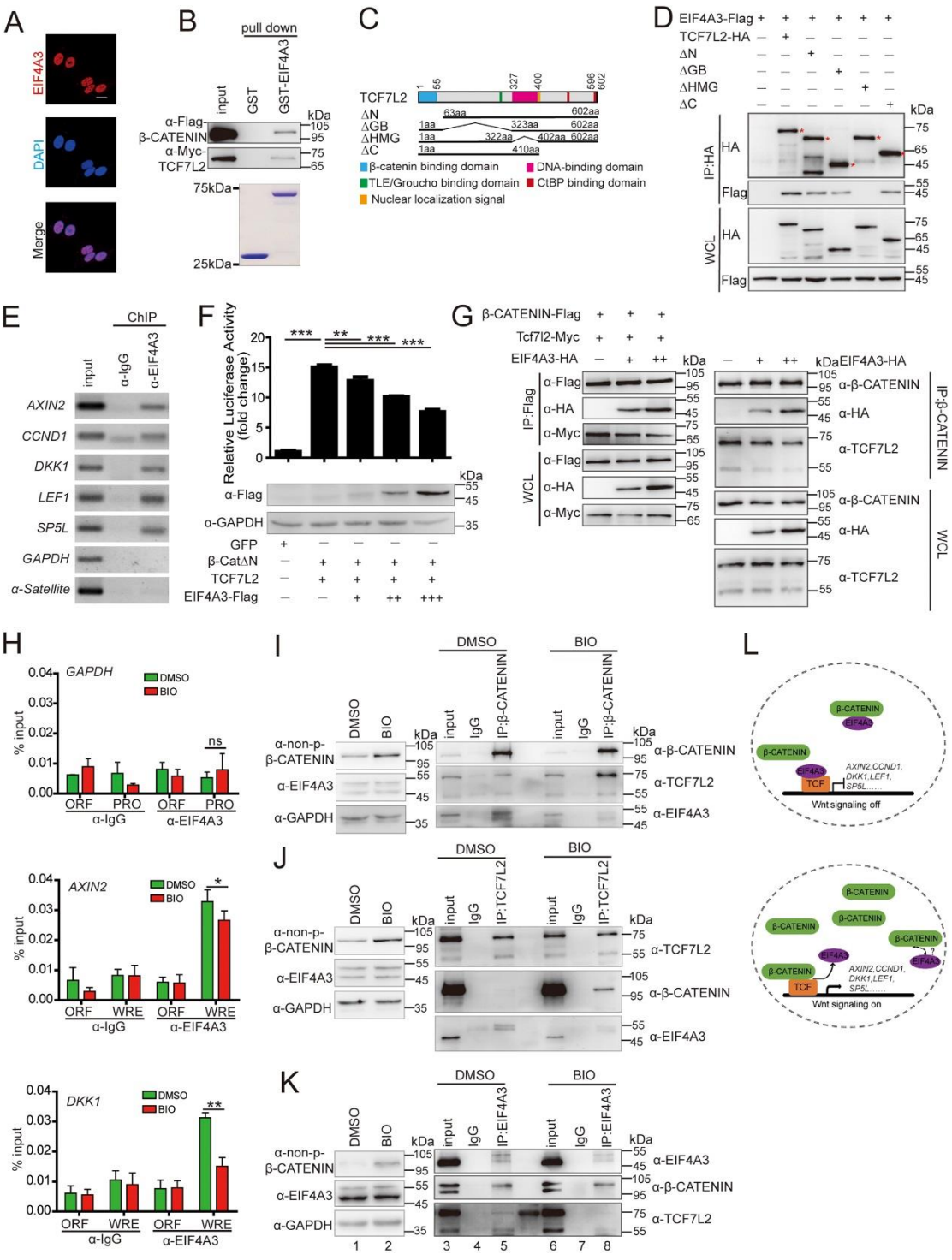

Fig. 3 EIF4A3 interfered with the β-CATENIN/TCF7L2 transcription activation complex. (A) Localization of EIF4A3 in HeLa cells, visualized by immunofluorescence (red) with an anti-EIF4A3 antibody. Nuclei (blue) were counterstained with DAPI. Scale bar: 20 μm. (B) EIF4A3 directly binds to β-CATENIN and TCF7L2. (C, D) Mapping of the region in the TCF7L2 responsible for the EIF4A3 interaction. Schematic diagram of human TCF7L2 protein domains was shown in (C). Various HA-tagged TCF7L2 deletion mutants were co-expressed with Flag-tagged EIF4A3 in HEK293T cells and cell lysates were subjected to

co-immunoprecipitation (D). *specific bands. (E) Endogenous EIF4A3 is associated with the promoters of the indicated Wnt target genes in HEK293T cells, as indicated by the ChIP assay. The promoters of *GAPDH* and *α-Satellite* were used as negative controls. (F) EIF4A3 represses β-CATENIN/TCF7L2-mediated transcriptional activity. (G) EIF4A3 impairs the interaction between β-CATENIN and TCF7L2. Left panel: HCT116 cells were co-transfected with tagged β-CATENIN and TCF7L2 along with various doses of EIF4A3. Right panel: EIF4A3 at various doses was transfected into HCT116 cells. Proteins were extracted from cell lysates, immunoprecipitated, and subjected to a western blot analysis using the indicated antibodies. (H) BIO treatment releases EIF4A3 from the indicated Wnt target genes in HEK293T cells, as indicated by ChIP assay. HEK293T cells were treated with DMSO or 1 μM BIO for 4 h and then cells were harvested for ChIP assay. The promoter of *GAPDH* was used as a negative control. WRE: Wnt response element; ORF: open reading frame; PRO: promoter region. (I, J, K) BIO treatment decreases the EIF4A3 in the β-CATENIN and TCF7L2 immunoprecipitant and similar response on β-CATENIN and TCF7L2 as in EIF4A3 immunoprecipitant. HEK293T cells were treated with DMSO or 1 μM BIO for 4 h, and then cells were harvested and proteins were extracted from cell lysates, immunoprecipitated, and subjected to a western blot analysis using the indicated antibodies to determine the interaction among EIF4A3, β-CATENIN, and TCF7L2 under different Wnt activity. (L) Working model for the role of EIF4A3 involved in the β-CATENIN/TCF complex. Values are represented as means ± S.E.M. (n = 3). *$p < 0.05$; **$p < 0.01$; ***$p < 0.001$, ns, not significant. Unpaired *t*-test, two-tailed.

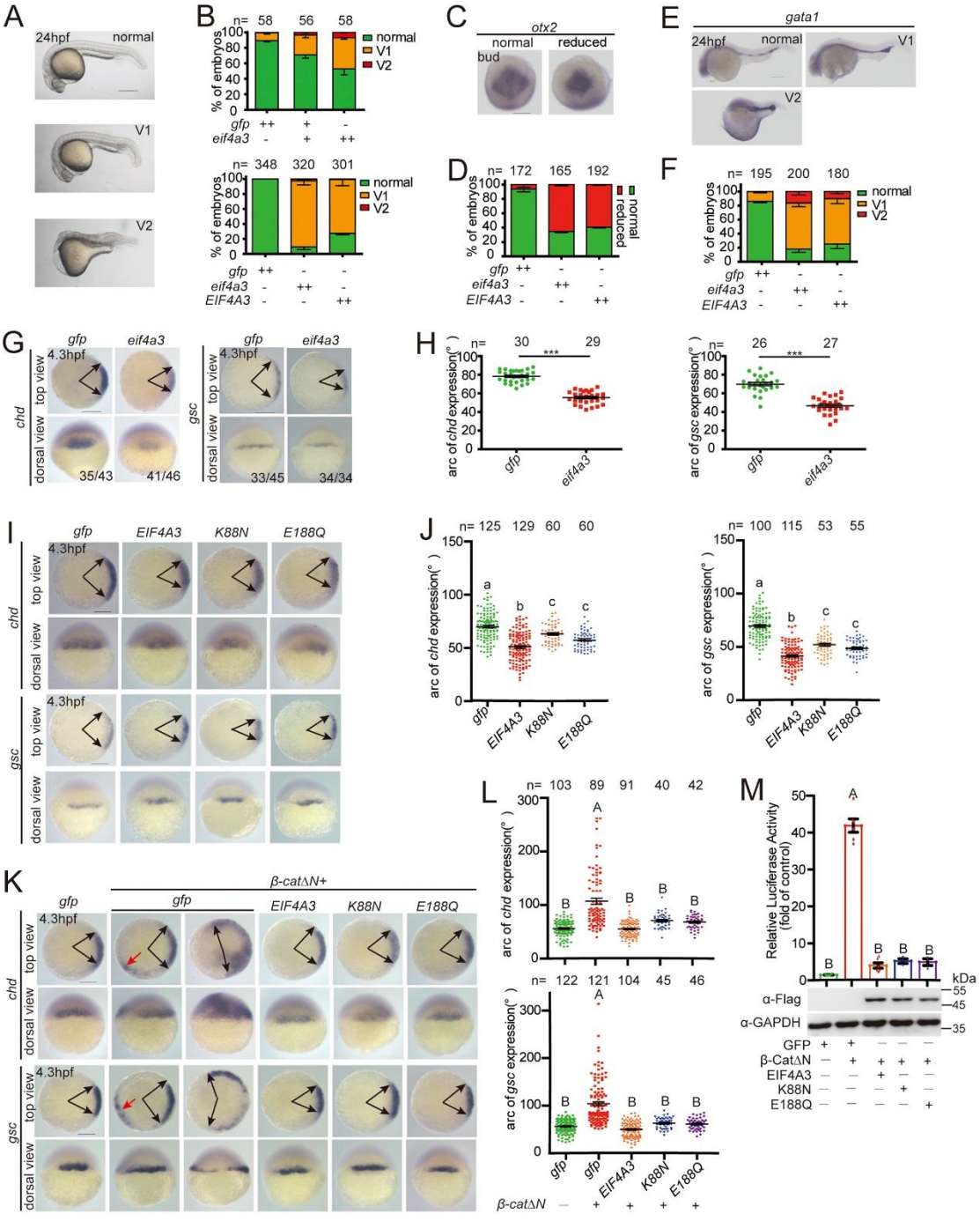

Fig. 4 Overexpression of EIF4A3/Eif4a3 in zebrafish resulted in ventralized phenotypes by inhibiting Wnt/β-catenin signals. (A) Overexpression of *EIF4A3/eif4a3* ventralizes zebrafish embryos. Classification of phenotypes at 24 hpf caused by the forced expression of *EIF4A3/eif4a3* mRNA. (B) Percentage of embryos in each category shown in A. The embryos were injected with 400 pg and 800 pg of *eif4a3* mRNA as well as 800 pg of *EIF4A3* mRNA. (C-F) Expression domain of *otx2* (C) and *gata1* (E) markers at indicated stages. Top views with dorsal to the downwards (C). (D, F) Percentage of embryos in each category shown in C and E. (G) Overexpression of *eif4a3* reduced the expression of indicated dorsal markers at 4.3 hpf. Embryos injected with 800 pg of *gfp* or *eif4a3* mRNA were raised to 4.3 hpf and then subjected to WISH analysis with indicated markers. Arrows indicate the edges of indicated

mRNA expression domains. (H) Quantification of the arc of marker expression shown in G. (I) Expression patterns of *chd* and *gsc* marker genes in zebrafish embryos injected with 800 pg of indicated mRNAs at 4.3 hpf. (J) Quantification of the arc of marker expression shown in I. (K) EIF4A3 mutants exhibit the inhibition on β-CatΔN activity *in vivo*. Expression patterns of *chd* and *gsc* marker genes in zebrafish embryos injected with 850 pg *gfp*, 50 pg *β-catΔN* plus 800 pg of each indicated mRNA at 4.3 hpf. Red arrow indicates the ectopic expression of *chd* and *gsc* on the ventral side. (L) Quantification of the arc of marker expression shown in K. (M) EIF4A3 mutants exhibit the inhibition on β-CatΔN activity *in vitro*. The indicated plasmid DNA was co-transfected with TOPFlash plasmid DNA into HCT116 cells and the luciferase activity was measured (n=3-6). The above results are from three independent experiments. The frequency of embryos with the indicated phenotypes is shown in the bottom right corner of each panel or the total embryo numbers are given at the top. All embryos are top views with dorsal to the right, and dorsal views with animal pole up. Values are means ± S.E.M. ***$p < 0.001$. Unpaired *t*-test, two-tailed. Groups labeled with different letters are significantly different from each other. lowercase letter, $p < 0.05$; capital letter, $p < 0.01$. One-way ANOVA followed by Tukey's post test. Scale bars: 200 μm.

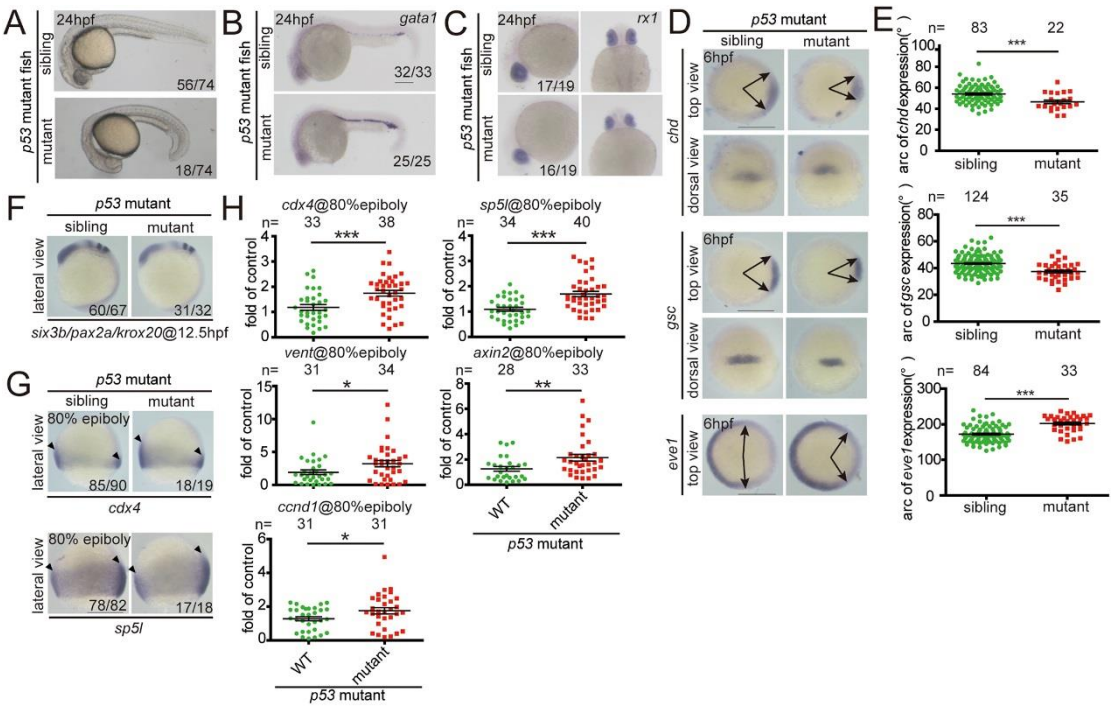

Fig. 5 Zygotic *eif4a3* mutant embryos exhibit ventralized phenotypes and increases Wnt activity. (A) Representative views of siblings and *eif4a3* mutants with a *p53*-deletion background at 24 hpf. (B, C) Expression of the indicated markers *gata1* and *rx1* in siblings and *eif4a3* mutants with the $p53^{-/-}$ background at 24 hpf. (D) Expression of the indicated dorsoventral markers in siblings and *eif4a3* mutants with the $p53^{-/-}$ background at 6 hpf. (E) Quantification of the arc of marker expression shown in D. (F) Expression of the indicated anteroposterior neural markers in siblings and *eif4a3* mutants with the $p53^{-/-}$ background at 12.5 hpf. Lateral views with the dorsal side to the right and animal pole up. (G) Expression of *cdx4* and *sp5l* in *eif4a3* mutants and siblings with the $p53^{-/-}$ background at 80% epiboly stage. Arrowheads indicate the edges of the indicated mRNA expression domains. Lateral views with the dorsal side to the right and animal pole up. (H) Depletion of *eif4a3* with the $p53^{-/-}$ background elevates the expression of the indicated Wnt direct target genes at 80% epiboly stage, as indicated by qRT-PCR analysis. Embryos are from three pairs of adult fishes. Embryos were raised to each indicated stage, subjected to the WISH analysis, photographed, and then genotyped in A-G. Each embryo was genotyped and subjected to qRT-PCR in H. Values are means ± S.E.M. *$p < 0.05$; **$p < 0.01$; ***$p < 0.001$. Unpaired *t*-test, two-tailed. Scale bars: 200 μm.

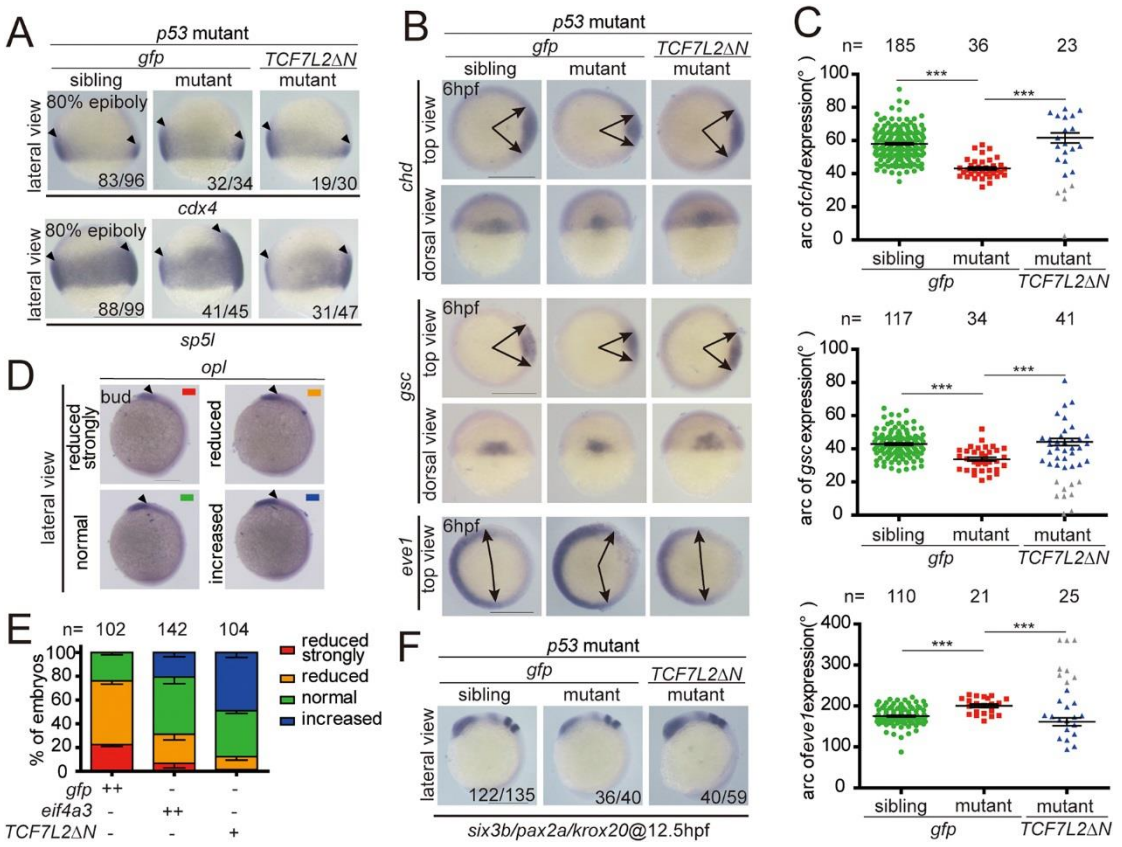

Fig. 6 Tcf7l2 repression counteracts the effects of *eif4a3* knockout in zebrafish embryos. (A) Expression areas of Wnt targets in indicated groups of embryos at 80% epiboly stage. (B) Expression of the dorsoventral markers in indicated groups at 6 hpf. (C) Quantification of the arc of marker expression shown in B. Note that a small number of mutant embryos within the *TCF7L2ΔN* mRNA injected groups showed more severe phenotypes in comparison with those of mutant embryos injected with *gfp* mRNA (labeled with grey). (D, E) Eif4a3 and TCF7L2ΔN rescue forebrain defects in *apc* mutants. Representative expression domain of the anterior neural marker, *opl*, in each indicated class of embryos at the bud stage (D) and quantification of each indicated class (E). One-cell stage embryos of $apc^{+/-}$ × $apc^{+/-}$ were injected with 200 pg of *gfp* or *eif4a3* mRNA or 50 pg of *TCF7L2ΔN* mRNA, raised to the bud stage, and subjected to the WISH analysis. Each embryo was photographed and then genotyped. (F) Expression of anteroposterior neural markers in each indicated group of embryos at 12.5 hpf. One-cell stage embryos were injected with 50 pg of *gfp* or *TCF7L2ΔN* mRNA, raised to the indicated stage, and subjected to WISH analysis. Each embryo was photographed and then genotyped. All embryos are lateral views with the dorsal to the right and anterior up, top views with dorsal to the right, and dorsal views with animal pole upwards. Embryos are from three pairs of adult fishes. Values are means ± S.E.M. ***$p < 0.001$. Unpaired *t*-test, two-tailed. Scale bars: 200 μm.

Fig. S1

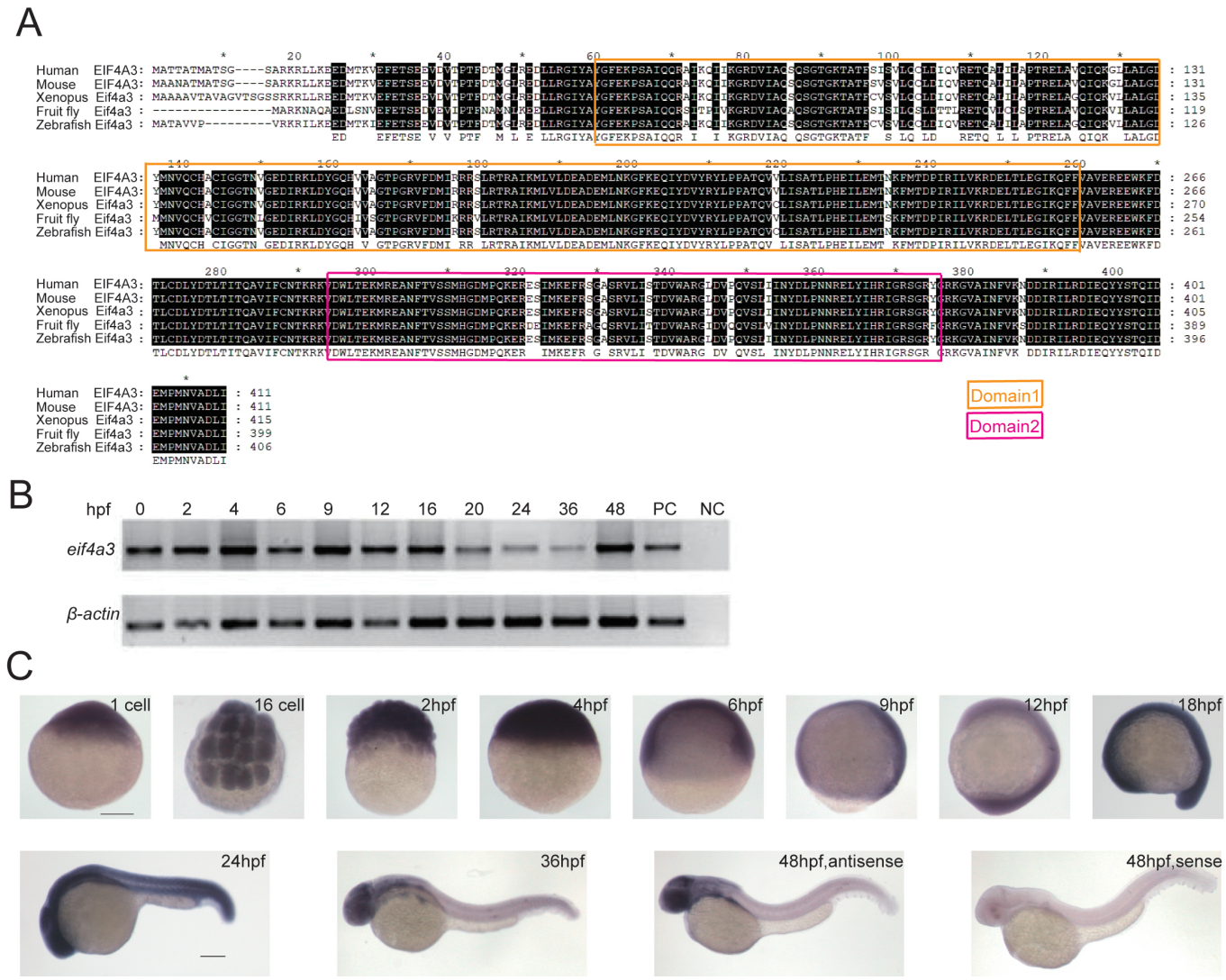

Fig. S1 Amino acid sequence alignment of EIF4A3/Eif4a3 and the spatiotemporal expression pattern of zebrafish *eif4a3*. (A) Amino acid sequence alignment of human, mouse, *Xenopus*, fruit fly, and zebrafish EIF4A3/Eif4a3. Identical amino acids are indicated in black. The accession numbers are as follows: human EIF4A3 P38919, mouse EIF4A3 Q91VC3, *Xenopus* Eif4a3 O42226, *D. melanogaster* Eif4a3 Q02748, and zebrafish Eif4a3 Q7ZVA6. (B) RT-PCR analysis of zebrafish *eif4a3* mRNA at the indicated embryonic stages. Numbers indicate different developmental stages as hours post fertilization (hpf). *β-actin* was used as an internal control. PC, positive control; NC, negative control. (C) Whole-mount *in situ* hybridization analysis of zebrafish *eif4a3* mRNA at the indicated stages. Panels are dorsal, top, or lateral views with the animal pole up or anterior side to the left. Scale bars: 200 μm.

Fig. S2

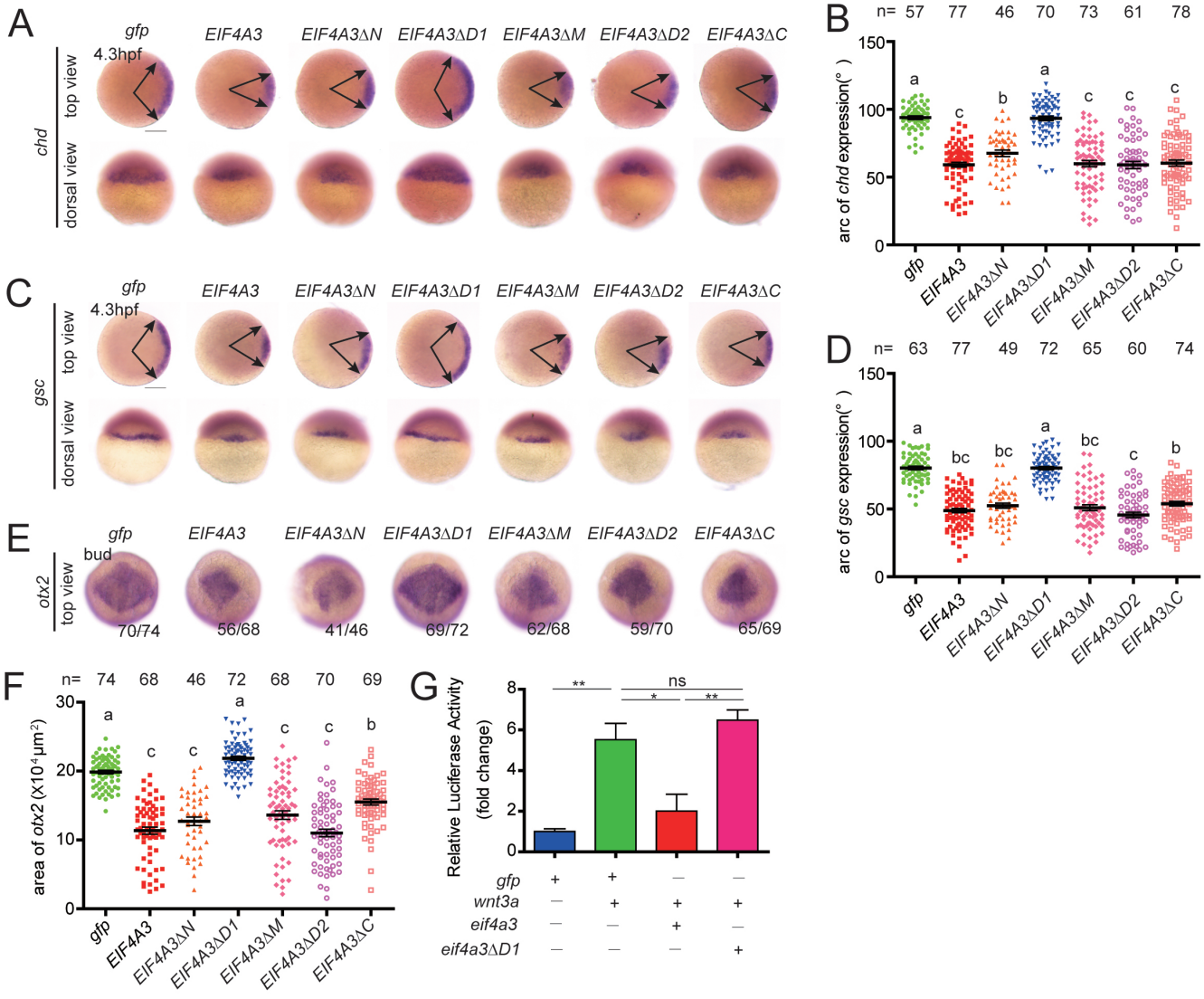

Fig. S2 The DEAD domain 1 of EIF4A3/Eif4a3 is required for Wnt inhibition. (A, C) Expression patterns of *chd* and *gsc* marker genes in zebrafish embryos injected with 800 pg of indicated mRNAs at 4.3 hpf. Arrows indicate the edges of indicated mRNA expression domains. Top views with dorsal to the right and dorsal views with animal pole upwards. (B, D) Quantification of the arc of marker expression shown in A and C. The total embryo numbers are given at the top. (E) Expression pattern of *otx2* marker gene in zebrafish embryos injected with 800 pg of each indicated mRNA at bud stage. Top views with dorsal to the downwards. The above results are from three independent experiments. The frequency of embryos with the indicated phenotypes is shown in the bottom right corner of each panel. (F) Quantification of the area of marker expression shown in E. The total embryo numbers are given at the top. (G) The DEAD domain 1 of zebrafish Eif4a3 is required for the inhibition of Wnt signaling *in vivo*. Embryos were injected with TOPFlash reporter DNA with the indicated mRNAs (800 pg of *gfp* mRNA, 10 pg of *wnt3a*, 10 pg of *wnt3a* plus 800 pg of *eif4a3* or *eif4a3ΔD1* mRNA). Values are means ± S.E.M. *$p < 0.05$; **$p < 0.01$; ns, not significant. Unpaired *t*-test, two-tailed. Or significance was calculated using One-way ANOVA followed by Tukey's post test (lowercase letter, p <0 .05). Scale bars: 200 μm.

Fig. S3

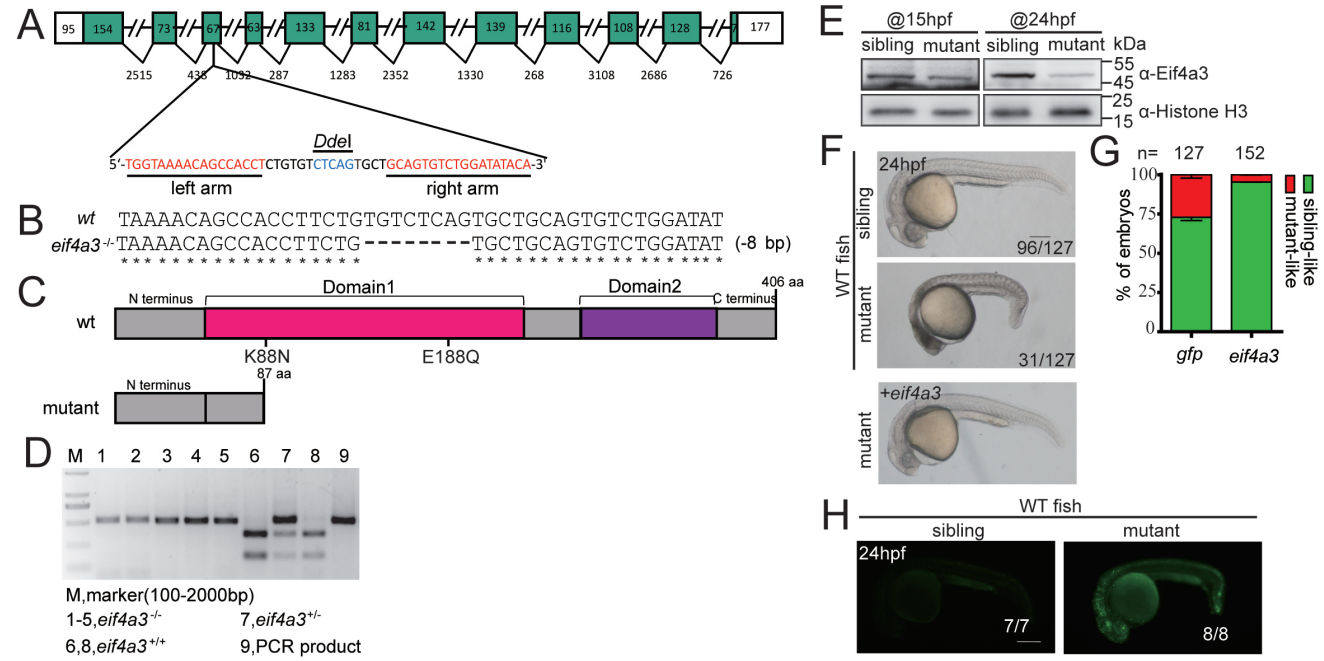

Fig. S3 Generation of zebrafish *eif4a3* knockout mutant by using TALEN system. (A) Schematic representation of the *eif4a3* locus. Exons are shown as boxes (filled green box, protein-coding region; open box, UTR). Introns are shown as lines. The left and right arms are highlighted in red. Restriction enzyme *Dde* I recognition sequences are highlighted in blue. (B) The sequence of the TALEN target site of wild-type (wt) and *eif4a3* mutant (*eif4a3*$^{-/-}$). The black dashed line indicates a deletion. (C) Schematic representation of the wild-type (upper) and mutant (lower) Eif4a3 protein structures. The position of each ATPase activity-dead mutant was shown. (D) Genotyping results by a restriction enzyme *Dde* I digestion assay. (E) The protein levels of Eif4a3 in sibling and mutant embryos at indicated stages. Proteins were extracted from the harvested zebrafish embryos at indicated stages and subjected to a western blot analysis using the indicated antibodies. (F) Representative views of siblings and zygotic mutants of *eif4a3* at 24 hpf. The frequency of embryos with the indicated patterns is shown in the bottom right corner of each panel. (G) The rescue effect of *eif4a3* mRNA in *eif4a3* mutants. One-cell stage embryos were injected with 50 pg of *gfp* or *eif4a3* mRNA. The phenotypes of injected embryos were scored following the criteria shown in F. The results are from three independent experiments, and the total embryo numbers are given at the top. (H) Acridine orange staining of sibling and zygotic mutant embryos at 24 hpf.

Fig. S4

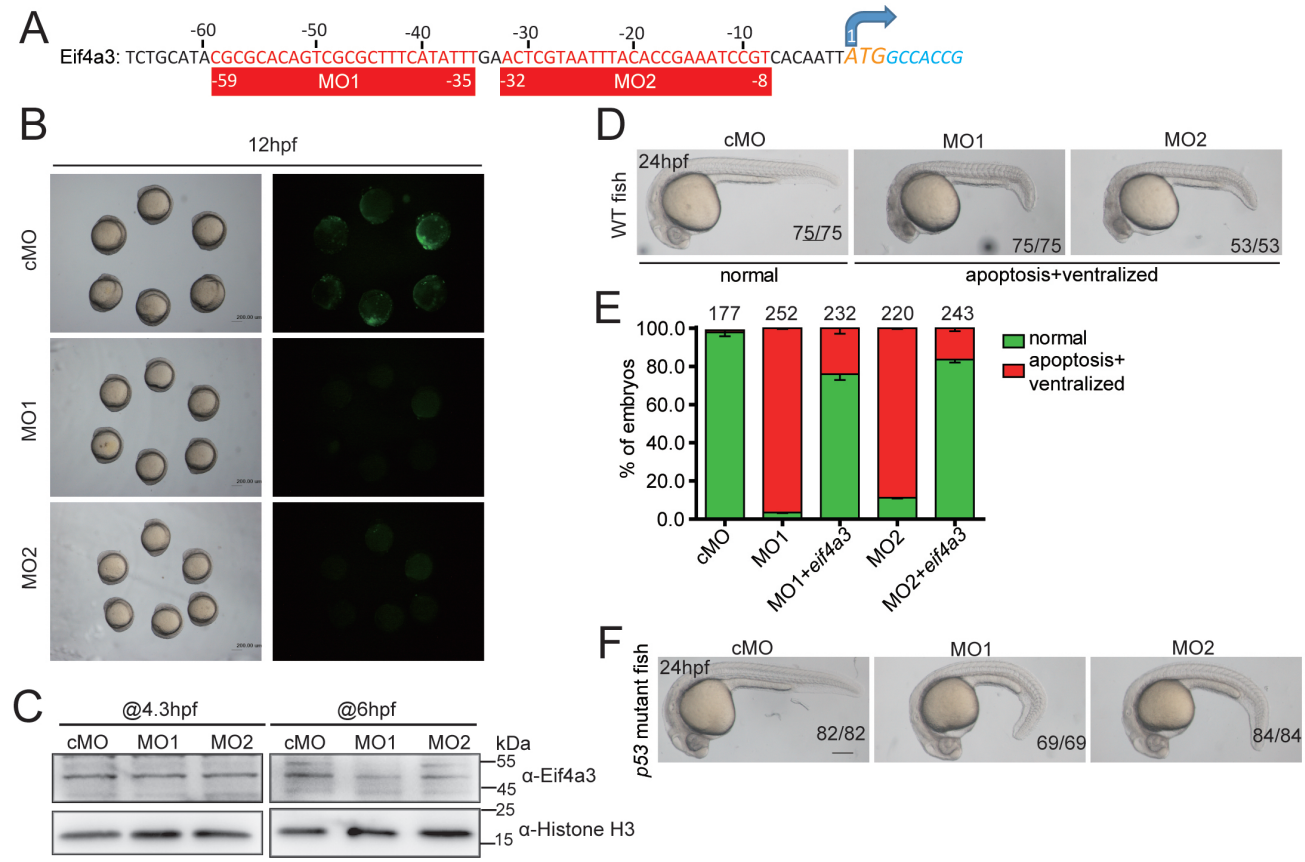

Fig. S4 Knockdown of *eif4a3* ventralizes embryos. (A) The targeting sequences of *eif4a3* translation-blocking MOs. (B) Effectiveness of the MO used. One-cell stage embryos were injected with the *eif4a3*-5'-UTR reporter plasmid DNA (50 pg) and control MO (cMO, 4 ng) or *eif4a3*-targeting MO (MO1 and MO2, 4 ng). Fluorescence micrographs of injected embryos at 12 hpf are shown. (C) The knockdown effect of MO1 and MO2 on the protein levels of Eif4a3 at indicated stages. Proteins were extracted from the harvested zebrafish embryos in the *p53*$^{-/-}$ background at indicated stages and subjected to a western blot analysis using the indicated antibodies. (D) Representative phenotypes caused by MO-mediated knockdown of *eif4a3* on wild-type embryos at 24 hpf. The results are from three independent experiments, and the frequency of embryos with the indicated pattern is shown in the bottom right corner of each group. (E) The neutralizing effects of Eif4a3 to *eif4a3* knockdown. One-cell stage embryos were injected with 4 ng of *eif4a3* MO1 or MO2 alone or 4 ng of *eif4a3* MO1 or MO2 plus 50 pg of *eif4a3* mRNA. The phenotypes of injected embryos were scored following the criteria shown in Fig. S4D. The results are from three independent experiments, and the total embryo numbers are given at the top. (F) Representative phenotypes caused by MO-mediated knockdown of *eif4a3* on *p53*$^{-/-}$ mutant embryos at 24 hpf. The results are from three independent experiments, and the frequency of embryos with the indicated pattern is shown in the bottom right corner of each group. Scale bars: 200 μm.

Fig. S5

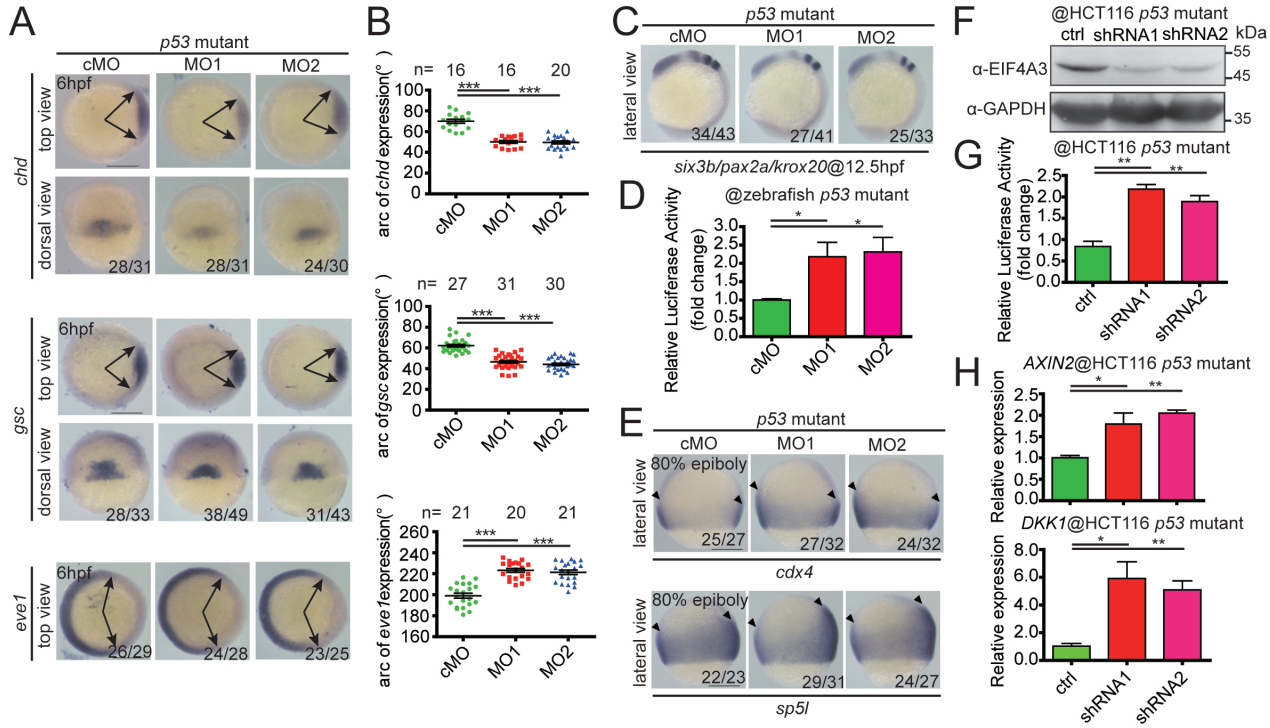

Fig. S5 Knockdown of *eif4a3* impairs dorsoventral patterning and anterior neuroectoderm development and depletion of EIF4A3/Eif4a3 increases Wnt activity. (A) Expression of the indicated dorsoventral markers in cMO-, and *eif4a3* MO-injected *p53*$^{-/-}$ mutant embryos at 6 hpf. Arrows indicate the edges of indicated mRNA expression domains. Top views with dorsal to the right and dorsal views with animal pole upwards and the frequency of embryos with the indicated pattern is shown in the bottom right corner of each group. (B) Quantification of the arc of marker expression shown in A. The total number of embryos of each group are given at the top. (C) Expression of the indicated anteroposterior neural markers in cMO- and *eif4a3* MO- injected *p53*$^{-/-}$ mutant embryos at 12.5 hpf. Lateral views with dorsal to the right and anterior up and the frequency of embryos with the indicated pattern is shown in the bottom right corner of each group. (D) Knockdown of *eif4a3* increased Wnt/β-catenin reporter activity. One-cell stage embryos were injected with TOPFlash reporter DNA together with cMO (6 ng), MO1 (6 ng), or MO2 (6 ng) and luciferase activity were measured at 6 hpf. (E) Effects of *eif4a3* knockdown on the expression of *cdx4* and *sp5l* at 80% epiboly stage as revealed by WISH. Arrowheads indicate the edges of the indicated mRNA expression domains. Lateral views with the dorsal side to the right and animal pole up. The results are from three independent experiments, and the frequency of embryos with the indicated pattern is shown in the bottom right corner of each group. (F) Effectiveness of EIF4A3 shRNA at the protein level in HCT116 cells with a *p53*$^{-/-}$ genetic background. ctrl, control shRNA. (G) Knockdown of EIF4A3 enhances endogenous Wnt signaling *in vitro*. The stable control or EIF4A3-depleted cells were transfected with TOPFlash reporter plasmids. (H) Knockdown of EIF4A3 increased the expression of the indicated Wnt direct target genes *in vitro*. Transcriptional levels were analyzed by qRT-PCR. Values are means±S.E.M. (n = 3). *$p < 0.05$; **$p < 0.01$; ***$p < 0.001$. Unpaired *t*-test, two-tailed. Scale bars: 200 µm.

Fig. S6

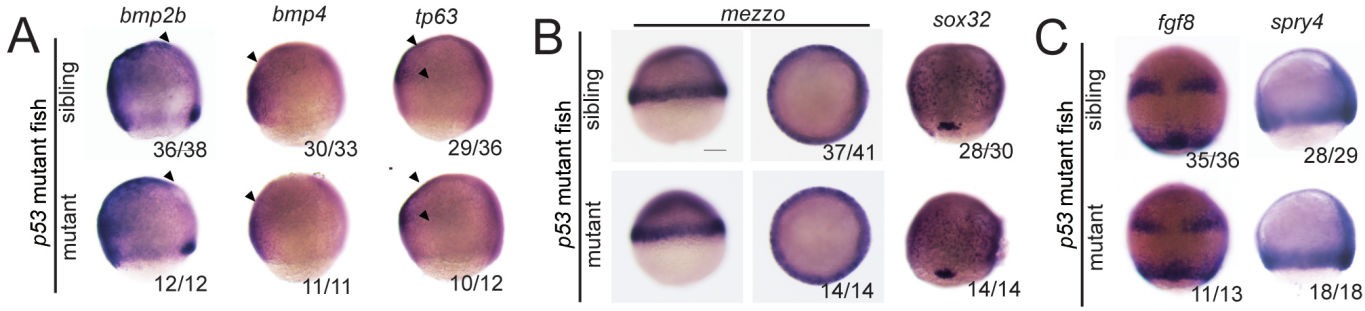

Fig. S6 Depletion of Eif4a3 in zebrafish embryos has little effect on Bmp, Nodal, or Fgf signaling pathways. (A) Expression of Bmp ligands, *bmp2b* and *bmp4*, and Bmp target *tp63* in indicated groups of embryos at 80% epiboly stage. Arrowheads indicate the edges of the indicated mRNA expression domains. (B) Expression of Nodal targets *mezzo* and *sox32* in indicated groups of embryos at 6 hpf and 80% epiboly stage, respectively. (C) Expression of Fgf ligand *fgf8* and Fgf target gene *spry4* in indicated groups of embryos at 90% and 80% epiboly stage. All embryos are lateral views with the dorsal to the right and anterior up, top views with dorsal to the right, and dorsal views with animal pole upwards. The results are from three independent experiments, and the frequency of embryos with the indicated pattern is shown in the bottom right corner of each group. Scale bars: 200 µm.

Fig. S7

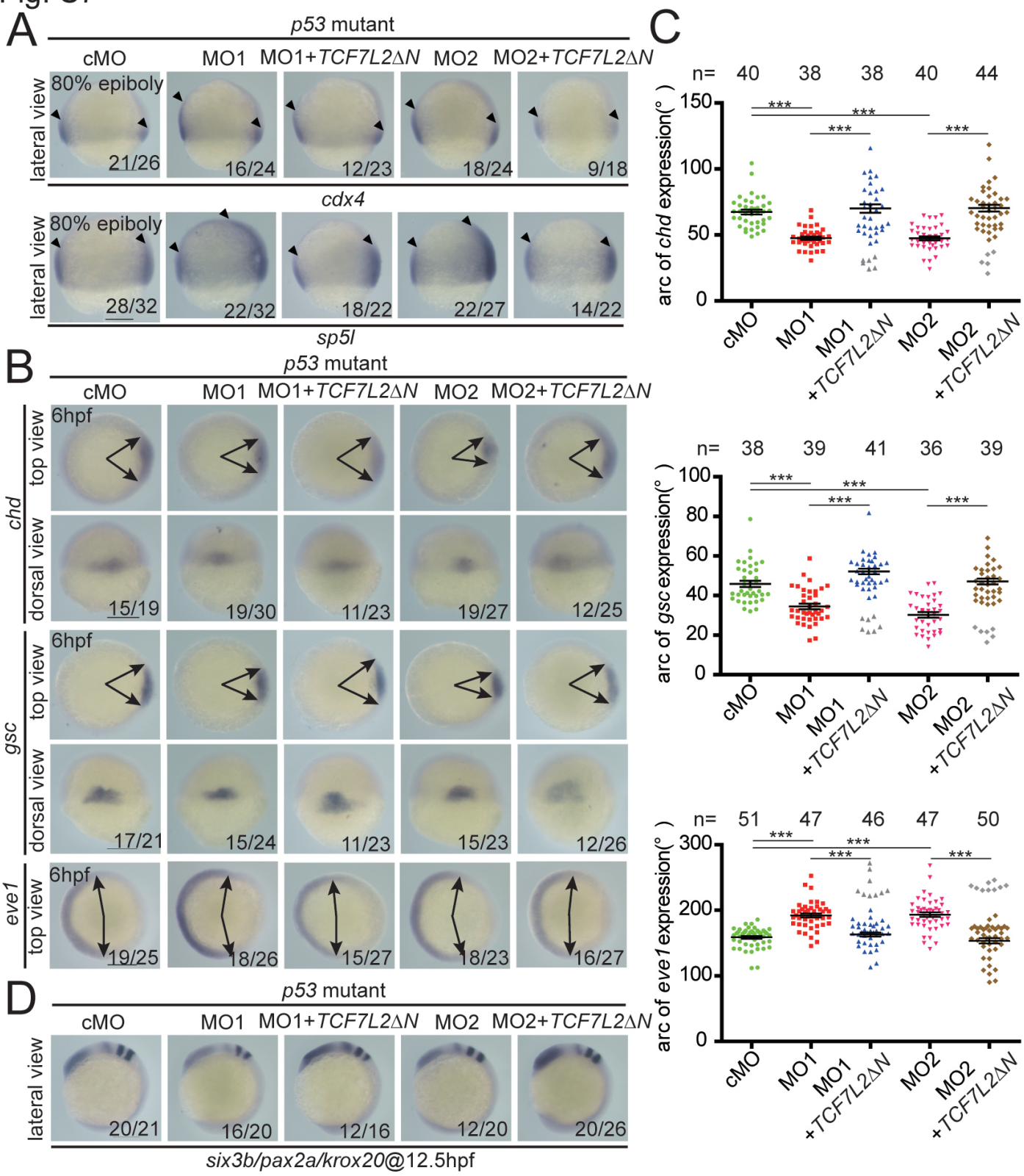

Fig. S7 Tcf7l2 repression counteracts the effects of *eif4a3* knockdown in zebrafish embryos. (A) Expression of Wnt direct targets in indicated groups of embryos at 80% epiboly stage. Arrowheads indicate the edges of the indicated mRNA expression domains. (B) Expression of the dorsoventral markers in indicated groups at 6 hpf. Arrows indicate the edges of mRNA expression domains. (C) Quantification of the arc of marker expression shown in B. Note that a small number of embryos within the *TCF7L2ΔN* co-injected groups showed more severe phenotypes in comparison with those of embryos injected with MOs only (Labeled with grey). (D) Expression of anteroposterior neural markers *six3b*, *pax2a*, and *krox20* mRNA in each indicated group of embryos at 12.5 hpf. The results are from three independent experiments. The frequency of embryos with the indicated patterns is shown in the bottom right corner of each panel or the total number of embryos of each group are given at the top. All embryos are lateral views with the dorsal side to the right and animal pole up, top views with dorsal to the right, and dorsal views with anterior up. Values are means ± S.E.M. ***$p < 0.001$. Unpaired *t*-test, two-tailed. Scale bars: 200 μm.

Table S1 Primers and sequence information.

Click here to download Table S1